

Discovery of highly potent benzimidazole derivatives as indoleamine 2,3-dioxygenase-1 (IDO1) inhibitors: from structure-based virtual screening to in vivo pharmacodynamic activity

Marta Serafini, Enza Torre, Silvio Aprile, Erika Del Grosso, Alessandro Gesù, Alessia Griglio, Giorgia Colombo, Cristina Travelli, Salvatore Paiella, Annalisa Adamo, Elena Orecchini, Alice Coletti, Maria Teresa Pallotta, Stefano Ugel, Alberto Massarotti, Tracey Piralì, and Silvia Fallarini

J. Med. Chem., **Just Accepted Manuscript** • DOI: 10.1021/acs.jmedchem.9b01809 • Publication Date (Web): 09 Mar 2020

Downloaded from pubs.acs.org on March 10, 2020

Just Accepted

“Just Accepted” manuscripts have been peer-reviewed and accepted for publication. They are posted online prior to technical editing, formatting for publication and author proofing. The American Chemical Society provides “Just Accepted” as a service to the research community to expedite the dissemination of scientific material as soon as possible after acceptance. “Just Accepted” manuscripts appear in full in PDF format accompanied by an HTML abstract. “Just Accepted” manuscripts have been fully peer reviewed, but should not be considered the official version of record. They are citable by the Digital Object Identifier (DOI®). “Just Accepted” is an optional service offered to authors. Therefore, the “Just Accepted” Web site may not include all articles that will be published in the journal. After a manuscript is technically edited and formatted, it will be removed from the “Just Accepted” Web site and published as an ASAP article. Note that technical editing may introduce minor changes to the manuscript text and/or graphics which could affect content, and all legal disclaimers and ethical guidelines that apply to the journal pertain. ACS cannot be held responsible for errors or consequences arising from the use of information contained in these “Just Accepted” manuscripts.

1
2
3
4
5
6
7
8
9
10
11
12
13
14
15
16
17
18
19
20
21
22
23
24
25
26
27
28
29
30
31
32
33
34
35
36
37
38
39
40
41
42
43
44
45
46
47
48
49
50
51
52
53
54
55
56
57
58
59
60

Discovery of highly potent benzimidazole derivatives as indoleamine 2,3-dioxygenase-1 (IDO1) inhibitors: from structure-based virtual screening to *in vivo* pharmacodynamic activity

Marta Serafini,^{1‡} Enza Torre,^{1‡} Silvio Aprile,¹ Erika Del Grosso,¹ Alessandro Gesù,¹ Alessia Griglio,¹ Giorgia Colombo,¹ Cristina Travelli,² Salvatore Paiella,³ Annalisa Adamo,⁴ Elena Orecchini,⁵ Alice Coletti,⁶ Maria Teresa Pallotta,⁵ Stefano Ugel,⁴ Alberto Massarotti,^{1*} Tracey Pirali^{1*} and Silvia Fallarini¹

¹ Department of Pharmaceutical Sciences; Università del Piemonte Orientale; Novara, 28100; Italy; ² Department of Pharmaceutical Sciences, Università degli Studi di Pavia, Pavia, 27100, Italy; ³ General and Pancreatic Surgery, Pancreas Institute; University of Verona, Verona, Italy 37134; ⁴ University Hospital and Department of Medicine, Section of Immunology; University of Verona, Verona, Italy 37126; ⁵ Department of Experimental Medicine; University of Perugia; Perugia, 06132; Italy; ⁶ Department of Medicine; University of Perugia, Piazza Lucio Severi 1, 06132 Perugia, Italy

1
2
3
4
5
6
7
8
9
10
11
12
13
14
15
16
17
18
19
20
21
22
23
24
25
26
27
28
29
30
31
32
33
34
35
36
37
38
39
40
41
42
43
44
45
46
47
48
49
50
51
52
53
54
55
56
57
58
59
60

ABSTRACT

In this study, a successful medicinal chemistry campaign that exploited virtual, biophysical and biological investigations led to the identification of a novel class of IDO1 inhibitors based on a benzimidazole substructure. This family of compounds is endowed with an extensive bonding network in the protein active site, including the interaction with pocket C, a region not commonly exploited by previously reported IDO1 inhibitors. The tight packing of selected compounds within the enzyme contributes to the strong binding interaction with IDO1, to the inhibitory potency at the low nanomolar level in several tumoral settings and to the selectivity towards IDO1 over TDO and CYPs. Notably, a significant reduction of L-Kyn levels in plasma, together with a potent effect on abrogating immunosuppressive properties of MDSC-like cells isolated from patients affected by pancreatic ductal adenocarcinoma, were observed, pointing to this class of molecules as a valuable template for boosting the antitumor immune system.

Introduction

Cancer immunotherapy is well-established as an effective clinical option for cancer treatment, alongside surgery, chemotherapy and radiation.¹ Indeed, immune checkpoint inhibitors (targeting CTLA-4 or PD-1/PD-L1 pathways) have become first-line therapies in advanced non-small cell lung cancer and melanoma.²

Nevertheless, this approach has shown substantial benefit to only some of the patients, while the rest do not respond, and even the patients that have initially a benefit might fail to respond in later stages. Mechanisms underlying resistance to cancer immunotherapy are complex and still under debate, but most of them rely on the immunosuppressive tumor microenvironment.³ Therefore, the search for novel strategies able to boost the antitumor immune system and make cancer

1
2
3 immunotherapy more versatile, durable and effective is an urgent need.⁴ In this context, among the
4
5 different combinatorial approaches that reverse tumor immunosuppression, the inhibition of
6
7 indoleamine 2,3-dioxygenase-1 (IDO1) has taken center stage.
8
9

10 IDO1 is an intracellular enzyme catalyzing the first, rate-limiting step of tryptophan (L-Trp)
11
12 catabolism resulting in the production of L-kynurenine (L-Kyn). IDO1 is expressed by primary
13
14 and metastatic tumor cells, intra-tumoral endothelial cells, immune cells of peri-tumoral stroma
15
16 and tumor-draining lymph nodes. This enzyme is a key mediator in the establishment of tumor
17
18 immune escape through different mechanisms.⁵ In particular, L-Trp degradation and L-Kyn
19
20 production induce: a) inhibition of mTOR1⁶ and activation of GCN2,⁷ resulting in dysfunction and
21
22 apoptosis of T effector cells; b) suppression of NK cell proliferation and functions;⁸ c)
23
24 differentiation and activation of regulatory T (Treg) cells,⁹ tolerogenic dendritic (DC)¹⁰ and
25
26 myeloid-derived suppressor cells (MDSCs);¹¹ d) tumor neovascularization.¹² Moreover, IDO1
27
28 expression and/or activity have been observed in several cancer types and are well correlated with
29
30 poor prognosis and low survival of patients.¹³
31
32
33
34

35 Recently, a better understanding of the molecular pathways linking L-Trp catabolism and tumor
36
37 immune tolerance has provided novel potential targets. In particular, L-Trp dioxygenase (TDO),
38
39 initially thought to be expressed only in liver, can be found in some other tumor types (*e.g.*
40
41 glioblastoma, breast cancer). Furthermore, preliminary *in vitro* studies revealed its involvement in
42
43 tumor induce immune tolerance,¹⁴ tumor cell resistance to *anoikis*, and metastatic prowess.¹⁵
44
45 Besides TDO, IDO2, whose functions are currently under investigation, is overexpressed in tumor
46
47 microenvironment, functionally enabling IDO1-dependent Treg and tolerogenic DC generation
48
49 and contributing to B cell-mediated autoantibody production. This latter aspect is an important
50
51 issue in the development of those types of cancer that rely upon B-cell to induce inflammation.¹⁶
52
53
54
55
56
57
58
59
60

1
2
3 Among the three L-Trp metabolizing enzymes, most attention has been paid to IDO1 and over the
4 last decades thousands of compounds have been reported as IDO1 selective inhibitors in cancer
5 immunotherapy.¹⁷ Only few have reached clinical trials, and none of these has been approved so
6 far, suggesting that the identification of potent and clinically useful IDO1 inhibitors is an open
7 challenge.¹⁸ Epacadostat (**1**, INCB024360, Figure 1),¹⁹ indoximod (**2**, 1-methyl-D-tryptophan,
8 Figure 1),²⁰ navoximod (**3**, NLG-919, Figure 1),²¹ EOS-200271 (**4**, PF-06840003, Figure 1)²² and
9 BMS-986205 (**5**, Figure 1) have been/are currently being tested in human clinical trials.

10
11
12 Based on promising results in Phase 1/2 studies, epacadostat has proceeded to Phase 3 trial
13 (ECHO-301) in combination with pembroluzimab in metastatic melanoma.²³ Recent results
14 coming from the pivotal Phase 3 of ECHO-301 have shown no indication that epacadostat provides
15 an increased benefit compared to pembrolizumab alone, questioning the effectiveness of IDO1
16 inhibitors.²⁴ This failure led to the interruption of other phase III trials and to reconsider whether
17 some elements had been neglected in the landscape of IDO1 inhibitors.²⁵ Among them, a nodal
18 point lies in the identification of biomarkers to stratify patients that respond better to this therapy.
19 In this regard, the detection of IDO1 expression and L-Kyn/L-Trp levels in tumor and metastatic
20 cells, as well as in peripheral blood mononuclear cells (PBMCs), would represent good prognostic
21 and response markers.²⁶

22
23
24 On a different note, availability of novel IDO1 inhibitors with different profiles in terms of PD and
25 PK properties may be necessary to restore hope to IDO1 inhibition and achieve clinical benefit.
26 Prompted by the challenge of discovering novel and effective IDO1 inhibitors, we have performed
27 a medicinal chemistry campaign that has started with a structure-based virtual screening approach
28 and has led to the identification of potent benzimidazole derivatives.

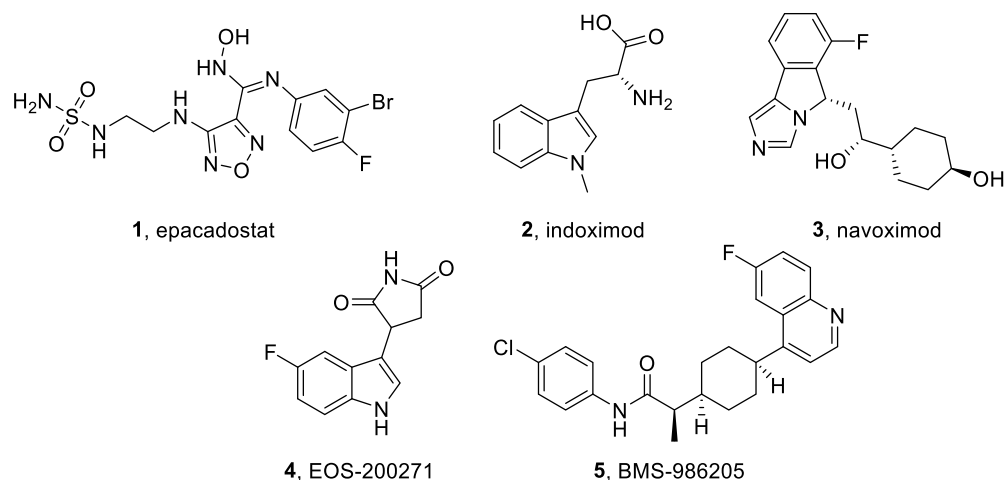


Figure 1. Chemical structures of IDO inhibitors that have reached clinical development.

Results

Structure-based virtual screening

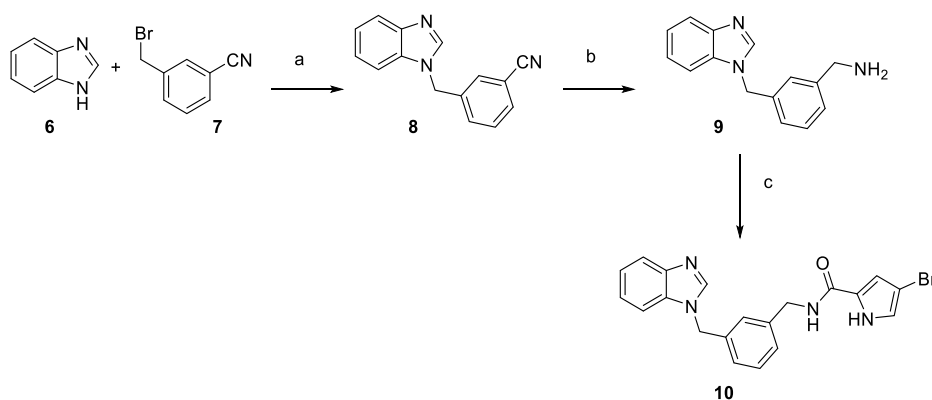
Most IDO1 inhibitors are characterized by a binding mode that exploits the coordination with heme iron and the interaction with pocket A, a large lipophilic pocket localized above the sixth coordination site of the iron-heme, and pocket B, a lipophilic area located at the binding site entrance (for a representation of IDO1 active site see Figure 2).^{18b} In 2018 our research group published a class of imidazothiazoles featuring a peculiar binding mode in the IDO1 active site, with the side chain protruding into an additional pocket, named C, where a crucial hydrogen bond is formed with Lys238.²⁷ We therefore integrated this novel information in a structure-based virtual screening. To this aim, all the bioactivity data of already known tested molecules were extracted and downloaded from scientific literature, following an approach already reported in our previous paper,²⁸ in order to validate the protocol. The database chosen for our screening purpose was ZINC15,²⁹ which contains readily purchasable and drug-like compounds. OMEGA2 program was used to generate a maximum of 500 conformations for each molecule with a root mean square

1
2
3 deviation (RMSD) of 0.8 Å between conformers. The processed database was docked into IDO1
4 active site (PDB structure 2D0T) with HYBRID³⁰ using default parameters, the results were sorted
5
6 using the predicted binding energy (Chemgauss4), and duplicates were removed. The top ranked
7
8 500 molecules were analyzed by visual inspection and by evaluating their pose in the active site
9
10 of IDO1. Among them, the first 50 commercially available molecules were selected and purchased
11
12 from eMolecules[®].³¹
13
14
15

16 17 18 **Evaluation of cellular inhibitory activity and identification of compound 10** 19

20 All the purchased molecules were tested for their IDO1 inhibition activity in a cell-based assay.
21
22 The melanoma derived A375 cell line was used as cellular model, since it expresses high levels of
23 IDO1 (RT-PCR) and L-Kyn (HPLC) when treated with recombinant human IFN- γ .^{27a} For the first
24
25 screening, A375 cells were untreated/treated with 10 μ M of each compound for 48 h and L-Kyn
26
27 levels were measured. A number of ten compounds out of 50 displayed an inhibitory activity >30%
28
29 at the tested concentration and in all cases cell viability was >85%, confirming that the observed
30
31 reduction in L-Kyn levels was not related to direct compound cytotoxicity. For the seven most
32
33 active compounds, the IC₅₀ value was determined in the cell-based assay (see Supporting
34
35 Information for the IC₅₀ values) and ranged from 4.4 μ M to 0.0016 μ M. The seven identified
36
37 compounds displayed no similarities in their structures and, among them, the most potent molecule
38
39 was **10** (Figure 2B), with an IC₅₀ value of 16 nM. We therefore decided to focus our efforts on this
40
41 hit, prompted by the fact that it was a novel chemotype (while other emerged compounds had
42
43 already been reported in the literature), that it was far more potent than the other identified
44
45 molecules (with at least a ten-fold lower IC₅₀ compared to the other emerged compounds), and that
46
47 no IDO1 inhibitor with similar structure had been previously described.
48
49
50
51
52
53
54
55
56
57
58
59
60

To validate our discovery, the hit was synthesized in our laboratory according to Scheme 1. The synthetic protocol afforded the desired amine **9** in two steps: substitution between 1*H*-benzo[*d*]imidazole and 3-(bromomethyl)benzonitrile and subsequent reduction of the aromatic nitrile **8**. Coupling between intermediate **9** and 4-bromo-1*H*-pyrrole-2-carboxylic acid provided **10** in good yield, highlighting the high synthetic feasibility displayed by our hit. The compound was re-tested at the same conditions and its potency was in accordance with the compound purchased from eMolecules[®].



Scheme 1. Re-synthesis of the hit compound **10**.

Reagents and conditions: (a) KOH, acetone, 60 °C, 4 h, 99%. (b) LiAlH₄, dry THF, 65 °C - rt, 18 h, 70%. (c) TEA, HOBt, EDCI, 4-bromo-1*H*-pyrrole-2-carboxylic acid, dry CH₂Cl₂, rt, 18 h, 50%.

Ligand binding experiments

In order to confirm target engagement of IDO1 by compound **10**, binding experiments were carried out using MicroScale Thermophoresis (MST) assays on recombinant human IDO1.³² Epacadostat (**1**) was used as positive control in this assay. As a result, a low dissociation constant was found for **10** ($K_d = 0.55 \pm 0.36 \mu\text{M}$; see Supporting Information), whereas a higher dissociation constant was determined for epacadostat (**1**, $K_d = 3.46 \pm 0.86 \mu\text{M}$, see Supporting Information). The K_d

1
2
3 value of compound **10** suggests that it does bind to IDO1, and therefore proves a direct target
4
5 engagement, accounting for the potent reduction of L-Kyn production in melanoma derived A375
6
7 cell line.
8
9

10 11 12 **Docking pose and SAR study of compound 10**

13
14
15
16 The docking pose of **10** (Figure 2) reveals a peculiar putative binding mode: the benzimidazole
17
18 group is accommodated in pocket A (Tyr126, Cys129, Val130, Phe163 and Phe164) and its
19
20 nitrogen coordinates the iron of the heme group. In contrast with other reported inhibitors, pocket
21
22 B (Phe226, Arg231 and Ser235) is not fully exploited since the phenyl ring is located in the
23
24 proximity of this pocket. Here, the carbonyl group establishes a hydrogen bond with Ser235. Two
25
26 additional hydrogen bonds are formed between the carboxylic moiety of the heme group and both
27
28 the amide and the pyrrole NH moieties. The long side-chain protrudes from the solvent-exposed
29
30 region of the active site towards pocket C, with the bromine that forms a putative halogen bond
31
32 with the close carbonyl group of Lys238.³³
33
34
35
36
37
38
39
40
41
42
43
44
45
46
47
48
49
50
51
52
53
54
55
56
57
58
59
60

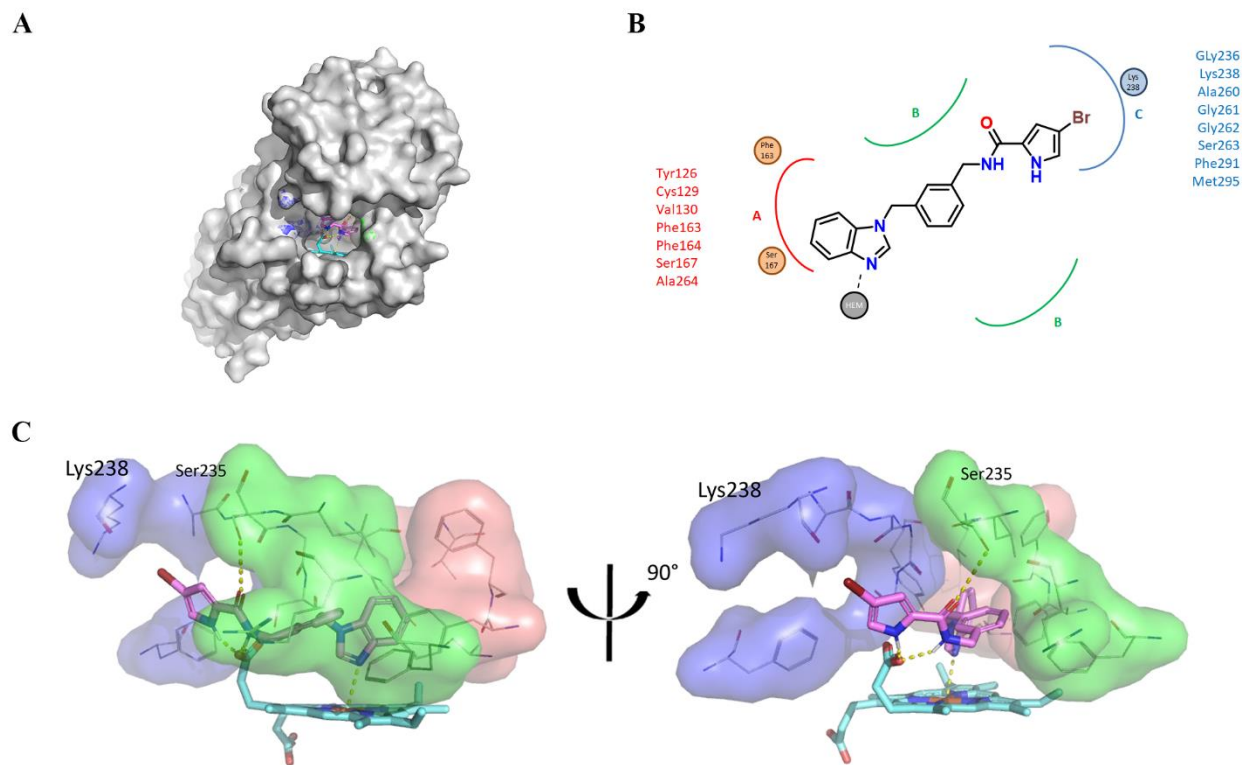
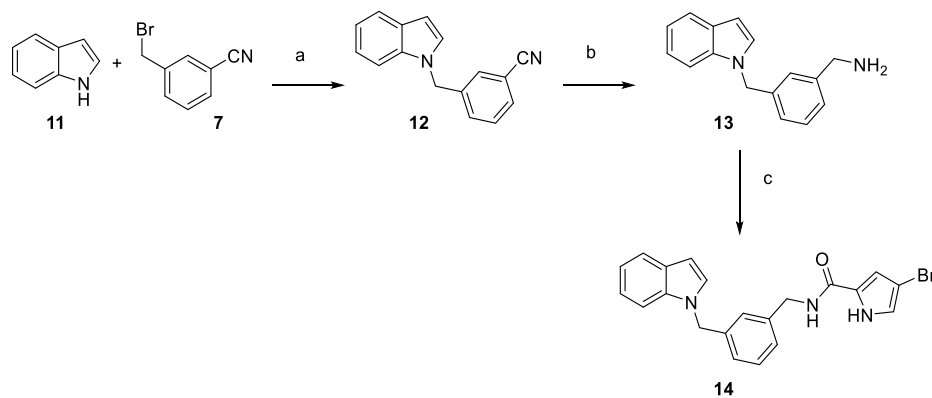


Figure 2. Structure and docking pose of the identified hit compound **10**. (A) Location of the binding region on IDO1 crystal structure (PDB id: 2D0T); (B) Schematic representation of predicted interactions of compound **10** within IDO1 binding pockets; (C) Docking pose of hit compound **10**. Aminoacids of pocket A, pocket B and pocket C are depicted in red, green and blue respectively. Heme group and compound **10** are depicted as cyan and pink sticks.

Starting from the scaffold of compound **10** and its putative binding mode, a SAR study was undertaken, with the aim of validating the predicted interactions by chemical modification of **10** and biological evaluation of the obtained analogues. The synthesized analogues were tested as IDO1 inhibitors in a cellular-based assay. The A375 cells unstimulated/stimulated with recombinant human IFN- γ were untreated/treated with 1 μ M of each compound for 48 h and L-Kyn levels were measured by HPLC.^{27a} For compounds showing an inhibitory activity >80% and

cell viability >80% the concentration/response curves were determined and IC₅₀ values calculated (Table 1).

First of all, in order to investigate the role of the nitrogen of the benzimidazole in the coordination with the iron of the heme group, compound **14** was synthesized. Substitution between 1*H*-indole and 3-(bromomethyl)benzonitrile and subsequent reduction of the nitrile group afforded the intermediate **13**, that, after coupling with 4-bromo-1*H*-pyrrole-2-carboxylic acid, yielded compound **14** (Scheme 2). As expected, the inhibitory activity was completely abolished (0% of inhibition, Table 1), confirming that the presence of the benzimidazole ring is crucial for the coordination with the heme group in the active site.

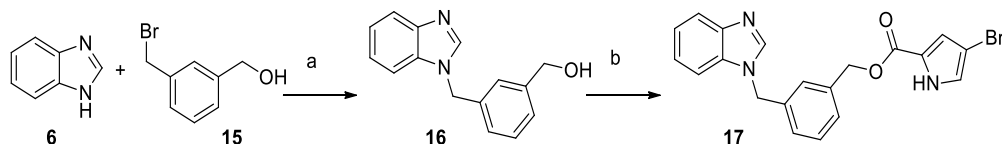


Scheme 2. Synthesis of compound **14**.

Reagents and conditions: (a) KOH, acetone, 60 °C, 4 h, 71%. (b) LiAlH₄, dry THF, 65 °C - rt, 18 h, 46%. (c) TEA, HOBt, EDCI, 4-bromo-1*H*-pyrrole-2-carboxylic acid, dry CH₂Cl₂, rt, 18 h, 54%.

Next, the role of the key hydrogen bond between the amide and the carboxylic moiety of the heme group was confirmed by the synthesis and evaluation of compound **17**, where the -NH- of the secondary amide is substituted with the -O- of the ester. **17** was prepared according to Scheme 3, starting from 1*H*-benzo[*d*]imidazole and (3-(bromomethyl)phenyl)methanol to afford intermediate

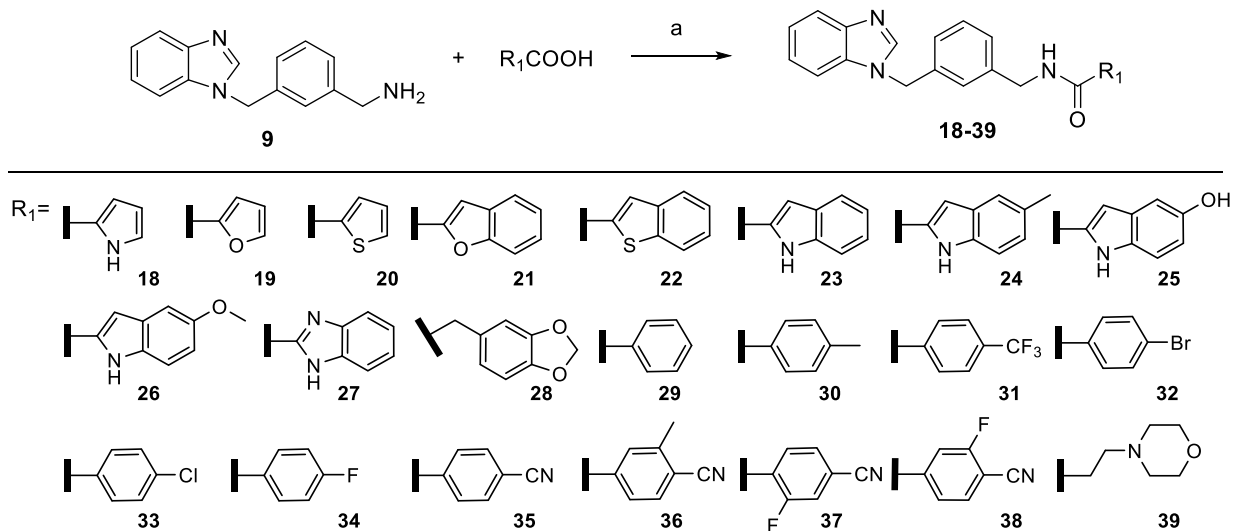
1
2
3 **16** that underwent esterification with 4-bromo-1*H*-pyrrole-2-carboxylic acid to provide the desired
4 compound. **17** is devoid of inhibitory activity at 1 μM , substantiating that the -NH- of the
5 secondary amide is involved in the formation of a pivotal hydrogen bond within the IDO1 active
6 site.
7
8 secondary amide is involved in the formation of a pivotal hydrogen bond within the IDO1 active
9 site.
10
11
12
13
14



23 **Scheme 3.** Synthesis of compound **17**.

24 Reagents and conditions: (a) KOH, acetone, 60 $^{\circ}\text{C}$, 2 h, 34%. (b) TEA, DMAP, EDCI, 4-bromo-
25 1*H*-pyrrole-2-carboxylic acid, dry CH_2Cl_2 , rt, 18 h, 40%.
26
27
28
29

30 Furthermore, the importance of the halogen bond between the bromine at 3 position on the pyrrole
31 ring and the close carbonyl group of Lys238 was investigated by the synthesis of compound **18**
32 that was obtained by coupling the amine **9** with the appropriate carboxylic acid, according to
33 Scheme 4. As suggested by the docking pose, the presence of the bromine contributes to the
34 binding as its removal leads to a decrease in activity (**18**, 72% of inhibition).
35
36
37
38
39
40
41
42
43
44
45
46
47
48
49
50
51
52
53
54
55
56
57
58
59
60



9
10
11
12
13
14
15
16
17
18
19
20
21
22
23
24
25
26
27
28
29
30
31
32
33
34
35
36
37
38
39
40
41
42
43
44
45
46
47
48
49
50
51
52
53
54
55
56
57
58
59
60

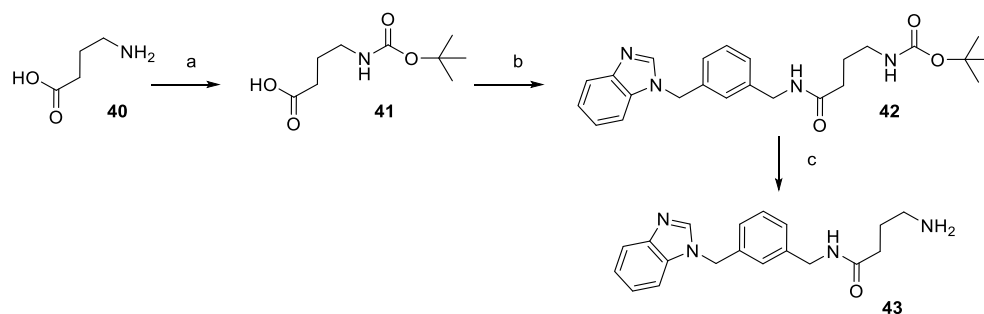
Scheme 4. Synthesis of compounds **18-39**.

Reagents and conditions: (a) TEA, HOBT, EDCI, dry CH₂Cl₂, rt, 18 h, 13-86%.

Finally, compounds **19** and **20**, displaying a furan and a thiophene ring, respectively, were prepared as described in Scheme 4 and evaluated with the aim of confirming the role of the -NH- of the pyrrole ring of **10** in establishing the hydrogen bond with the carboxylic moiety of the heme group. As expected, a decrease in the inhibitory activity occurs in both cases (**19** and **20**, 25% and 62% of inhibition, respectively).

Besides the above SAR study, in order to investigate the role of the 4-bromopyrrole moiety placed in pocket C and further improve the potency of compound **10**, a series of analogues was *in silico*-designed and synthesized (**21-39**, **43**, **46**, **47**). To this aim, about 44,000 purchasable carboxylic acids have been virtually combined with compound **9**, and the resulted library of candidates has been screened in the IDO1 active site, using the same virtual screening procedure described before. Compounds have been ranked according to their binding energies in the protein, as well as their drug-like profiles. The virtual candidates that displayed the highest score have been selected for synthesis.

By coupling amine **9** with different carboxylic acids (Scheme 4), 19 benzimidazoles have been obtained in good to excellent yields (**22-24**, **26-39**, **43**), with only two exceptions (**21**, **25**) showing poor yield (Table 1). For the synthesis of compound **43** protection and deprotection of the additional amine group were necessary, according to Scheme 5.



Scheme 5. Synthesis of compound **43**.

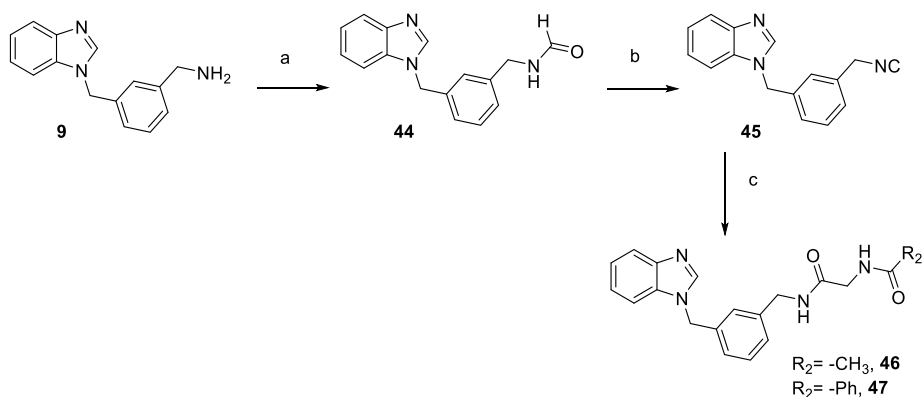
Reagents and conditions: (a) 2 M aq. NaOH, Boc₂O, THF, 16 h, 86%. (b) Compound **9**, TEA, HOBt, EDCI, dry CH₂Cl₂, rt, 18 h, 57%. (c) CF₃COOH, dry CH₂Cl₂, 0 °C, 30 min, 71%.

Benzofuran **21** shows an IC₅₀ value of 413 nM, while benzothiophene (**22**) provides a lower inhibitory activity (77% of inhibition). If pyrrole is fused with both a non-substituted (**23**) or a substituted (**24**, **25**) phenyl ring, the activity is retained (IC₅₀ = 72, 636, 781 nM, respectively), while when a 5-methoxy-1*H*-indole substituent is present (**26**) a significant cytotoxicity is observed (55% of viability at 1 μM). Finally, the benzimidazole **27** is well tolerated (IC₅₀ = 407 nM), while a benzodioxolane ring is not (**28**, 5% of inhibition).

The SAR study reveals that for the analogues displaying a phenyl ring at the R₁ position (**29-38**), when unsubstituted, the inhibitory activity is lost (**29**, 32% of inhibition). Electron-donating (**30**) and electron-withdrawing groups such as trifluoromethyl (**31**), bromine (**32**), chlorine (**33**) and fluorine (**34**) at position 4' reduce potency compared to **10**. On the other hand, compound **35**

1
2
3 displaying a cyano group at position 4' retains a good potency ($IC_{50} = 90$ nM), while the activity
4 is lower when other substituents are added on the -CN substituted phenyl ring (**36**, **37**, **38**).

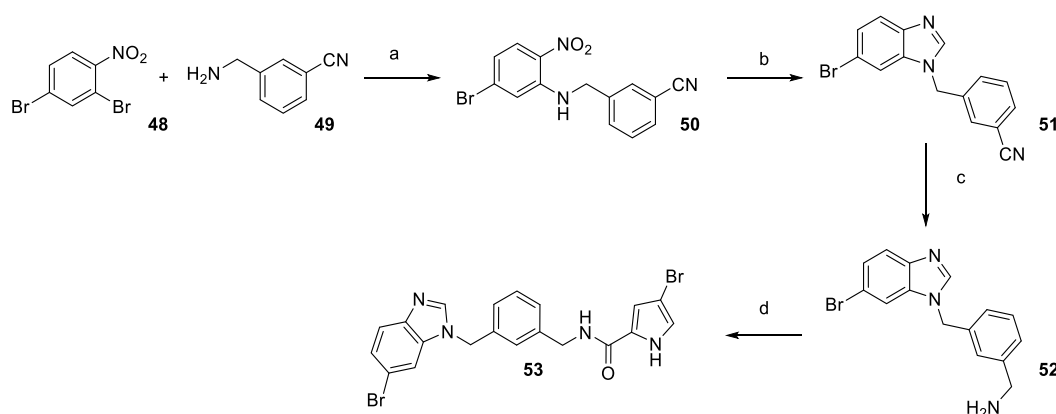
5
6
7 Compounds **46** and **47** have been synthesized by using Ugi multicomponent reaction (MCR) and
8 exploiting ammonium chloride as a nitrogen source. The required isocyanide **45** has been
9 synthesized starting from amine **9** that was formylated and dehydrated. Then, two MCRs have
10 been set up using isocyanide **45**, paraformaldehyde, ammonium chloride and acetic or benzoic
11 acid, yielding compounds **46** and **47**, respectively (Scheme 6). The yields of both reactions were
12 very poor (30-32%), not surprisingly since it is well known that Ugi MCR does not work well
13 when ammonia is employed as nitrogen source.³⁴ The introduction of a polar moiety (**39**, **43**) at R_1
14 position or a peptidic substructure (**46**, **47**) in the side chain are not tolerated, inducing a drop in
15 activity.
16
17
18
19
20
21
22
23
24
25
26
27
28
29
30
31
32
33
34
35
36
37
38
39
40
41
42
43
44
45
46
47
48
49
50
51
52
53
54
55
56
57
58
59
60



Scheme 6. Synthesis of compounds **46** and **47**.

Reagents and conditions: (a) Ac_2O , $HCOOH$, 3 h, 98%. (b) TEA, $POCl_3$, dry CH_2Cl_2 , 0 °C, 2.5 h, 44%. (c) NH_4Cl , CH_2O , TEA, R_2COOH , MeOH, H_2O , 65 °C, 8 h, 30-32%.

1
2
3 Since pocket A is not completely occupied by compound **10** and other reported IDO1 inhibitors
4 display halogen atoms to increase the affinity with this buried pocket, a bromine atom was
5 introduced at position 6 of the benzimidazole core with the aim of improving the affinity with
6 pocket A. Compound **53** was synthesized following the synthetic route outlined in Scheme 7. The
7 desired amine **52** was prepared *via* a three-step procedure: nucleophilic aromatic substitution,
8 cyclization and reduction of the nitrile group (Scheme 7).
9
10
11
12
13
14
15
16
17
18
19
20



34 **Scheme 7.** Synthesis of compound **53**.

35
36 Reagents and conditions: (a) K_2CO_3 , DMSO, 72 °C, 16 h, 13%. (b) formic acid, Fe, 85 °C, 16 h,
37
38 69%. (c) $LiAlH_4$, dry THF, rt, 16 h, 40%. (d) TEA, HOBt, EDCl, dry CH_2Cl_2 , rt, 18 h, 39%.
39
40
41
42

43 Compound **53** shows an IC_{50} value of 19 nM, but its chemical instability together with the lack of
44 improvement in ADME properties compared to the hit compound (data not shown) have prompted
45 us to discard the compound.
46
47
48
49

50 Taking into consideration all these data, the main findings are represented in Figure 3 and the
51 compounds **10**, **23** and **35** that display no significant cytotoxicity and IC_{50} values of 16, 72 and 90
52
53 nM, respectively, have been selected for further evaluation.
54
55
56
57
58
59
60

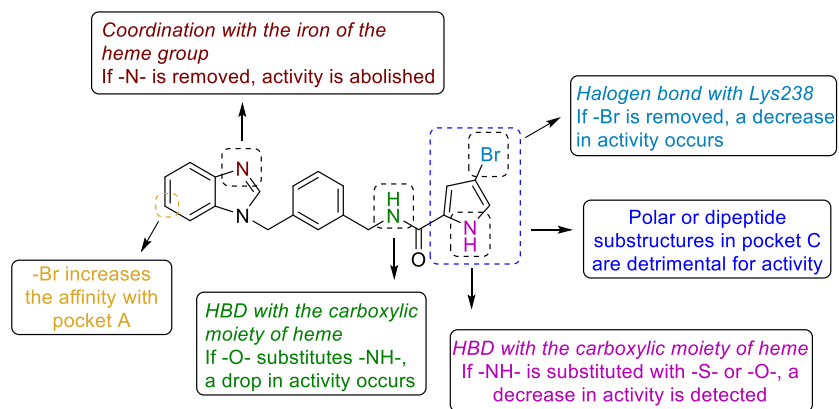
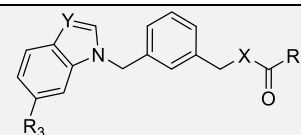
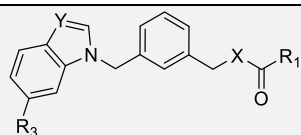
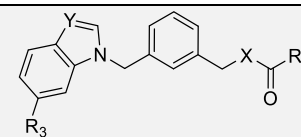
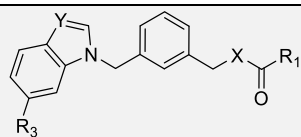


Figure 3. Graphical representation of SAR study around compound **10**.

Table 1. SAR study around compound **10**.

Cpd,	X	Y	R ₁	R ₃	Cell viability (%) @ 1 μM ± SD	IDO cellular assay inhibition (%) @ 1 μM	IC ₅₀ (nM)	Cpd, Yield (%)	X	Y	R ₁	R ₃	Cell viability (%) @ 1 μM ± SD	IDO cellular assay inhibition (%) @ 1 μM	IC ₅₀ (nM)
1	-	-	-	-	97 ± 2.5	92 ± 3.6	7.7	29 , 54%	NH	N		H	98 ± 2	32 ± 15	-
10 , 50%	NH	N		H	100 ± 0.5	96 ± 0.2	16	30 , 69%	NH	N		H	94 ± 3	88 ± 2.1	327
14 , 54%	NH	H		H	100 ± 0	0 ± 4	-	31 , 82%	NH	H		H	97 ± 3	81 ± 4.9	-
17 , 40%	O	N		H	100 ± 0	0 ± 2	-	32 , 77%	NH	N		H	96 ± 4	98 ± 1.4	134
18 , 62%	NH	N		H	94 ± 6	72 ± 2.1	-	33 , 60%	NH	N		H	96 ± 4	99 ± 0	477
19 , 65%	NH	N		H	100 ± 0	25 ± 11.4	-	34 , 78%	NH	N		H	89 ± 7	88 ± 7.1	961

Cpd,	X	Y	R ₁	R ₃	Cell viability (%) @ 1 μM ± SD	IDO cellular assay inhibition (%) @ 1 μM	IC ₅₀ (nM)	Cpd,	X	Y	R ₁	R ₃	Cell viability (%) @ 1 μM ± SD	IDO cellular assay inhibition (%) @ 1 μM	IC ₅₀ (nM)
Yield (%)								Yield (%)							
20 , 78%	NH	N		H	98 ± 1	62 ± 9.9	-	35 , 77%	NH	N		H	100 ± 1	88 ± 6.9	90
21 , 37%	NH	N		H	100 ± 0	91 ± 4	413	36 , 51%	NH	N		H	94 ± 1	44 ± 16.9	-
22 , 52%	NH	N		H	88 ± 1	77 ± 1.2	-	37 , 60%	NH	N		H	99 ± 1	37 ± 0	-
23 , 54%	NH	N		H	99 ± 4	94 ± 3.5	72	38 , 48%	NH	N		H	100 ± 0	32 ± 14.5	-
24 , 49%	NH	N		H	99 ± 1	90 ± 7.5	636	39 , 55%	NH	N		H	100 ± 1	0 ± 0	-
25 , 13%	NH	N		H	99 ± 1	71 ± 15.5	781	43 , 71%	NH	N		H	100 ± 0	0 ± 0	-
26 , 56%	NH	N		H	55 ± 11	-	-	46 , 30%	NH	N		H	100 ± 0	0 ± 0	-
27 , 86%	NH	N		H	100 ± 0	83 ± 10.6	407	47 , 32%	NH	N		H	99 ± 0	13 ± 0.7	-



1
2
3
4
5
6
7
8
9
10
11
12
13
14
15
16
17
18
19
20
21
22
23
24
25
26
27
28
29
30
31
32
33
34
35
36
37
38
39
40
41
42
43
44
45
46
47

Cpd, Yield (%)	X	Y	R ₁	R ₃	Cell viability (%) @ 1 μM ± SD	IDO cellular assay inhibition (%) @ 1 μM	IC ₅₀ (nM)	Cpd, Yield (%)	X	Y	R ₁	R ₃	Cell viability (%) @ 1 μM ± SD	IDO cellular assay inhibition (%) @ 1 μM	IC ₅₀ (nM)
28 , 84%	NH	N		H	96 ± 3	5 ± 6.4	-	53 , 39%	NH	N		Br	99 ± 1	98 ± 1.7	19 nM

Profiling of compounds **10**, **23** and **35**

IDO1 and TDO selectivity

The three selected compounds were tested in a mastocytoma cell line stably expressing mouse IDO1 (P1.IDO1) or TDO (P1.TDO) in order to evaluate their selectivity. To this aim, cells P1.IDO1 and P1.TDO were treated with different dilutions of **10**, **23** and **35** for 16 h and L-Kyn secretion in cell culture supernatants was detected by HPLC analysis. In these settings, the compounds behaved as selective inhibitors of IDO1 against TDO at 1 μM , yet when the concentration was increased up to 10 μM , an inhibition of TDO was observed to some extent. We measured the IC_{50} value of each compound in the two cell lines and we found that IC_{50} of compound **10** is 12.7 nM in P1.IDO1 and 5.46 μM in P1.TDO. Moreover, for **23** IC_{50} is 9.3 nM in P1.IDO1 and 13.2 μM in P1.TDO, whereas for **35** IC_{50} is 111.7 nM and 32.3 μM , respectively, suggesting a high selectivity of the three compounds towards IDO1 over TDO .

IDO1 inhibitory activity in a set of different tumoral cell lines

Compared to epacadostat (**1**, Figure 1), compound **10** showed a very similar activity in the A375 cell line, with IC_{50} values of 7.7 nM and 16 nM, respectively. The cellular potency of **10** in inhibiting L-Kyn production was further investigated using several human cell lines, including cervical cancer derived HeLa cells, lung cancer derived LXF-289 cells, breast cancer derived MCF-7 cells, liver cancer derived HepG2 cells and pancreas cancer derived DAN-G cells. As shown in Table 2, compound **10** is able to inhibit L-Kyn production in most cell lines with potency comparable with that observed in A375 cell line, suggesting that it effectively inhibits IDO1 enzyme activity regardless of cell source. Compared to the other cell lines, in the pancreatic derived DAN-G cells **10** showed an IC_{50} value of one order of magnitude greater ($0.605 \mu\text{M} \pm$

0.0626) than those observed in the other cells. This result could be ascribed to the concomitant expression of other Trp degrading enzymes such as TDO, as suggested by Western Blot analysis (data not shown), or IDO2, and to the fact that, as reported above, compound **10** is a selective inhibitor of IDO1.

Table 2. Potency of compound **10** on different cell lines.

Cell line	IC ₅₀ (μM)
A375	0.016 ± 0.0004
HeLa	0.064 ± 0.0018
LXF-289	0.014 ± 0.0002
MCF-7	0.021 ± 0.0006
HepG2	0.043 ± 0.0016
DAN-G	0.605 ± 0.0626

On the same note, the activity of **23** and **35** was measured on human breast derived MCF-7 and human pancreas derived DAN-G cell lines as *in vitro* models. As shown in Table 3, the IC₅₀ values obtained in MCF-7 cell line were slightly increased for both compounds (0.083 μM ± 0.005 and 0.11 μM ± 0.23 for **23** and **35**, respectively). As observed for compound **10**, the IC₅₀ values measured in DAN-G cell line were higher than those observed in A375 cell line for both compounds, in particular of one and two order of magnitude greater for compounds **23** and **35**, respectively.

Table 3. Potency of compounds **23** and **35** on different cell lines.

Compound Cell line	IC₅₀ (μM) 23	IC₅₀ (μM) 35
A375	0.072 ± 0.002	0.09 ± 0.006
MCF-7	0.083 ± 0.005	0.11 ± 0.23
DAN-G	0.14 ± 0.007	1.94 ± 0.23

Molecular dynamics

The docking results of compounds **10** (Figure 2), **23** and **35** (see Supporting Information) were further analyzed with Molecular Dynamics (MD) simulations using Desmond package.³⁵ The MD of IDO1/compound complexes were simulated for 100 ns at 300 K using a standard protocol. The protein structure was stabilized, as shown in the RMSDs for both the IDO1 C α and the ligand (see Supporting Information). In the MD simulation the benzimidazole moiety of **10** is stabilized in pocket A, where it is able to interact, for the majority of time, with the amino acidic residues of Phe163 and Tyr126, as well as with the heme group. This behavior is consistent with the docking results, as well as the contacts near the pocket B, such as with Arg231. On the other hand, the hydrogen bond interaction with Ser235 occurs for only the 50% of the simulation time. The pyrrole group of **10** makes interactions with the amino acids in pocket C, that are present for up to 10% of the simulation time. The conformation of hIDO1 changes during the MD, and in this relaxed/dynamic situation the side-chain of **10** that is more exposed to the solvent is shifted near the pocket B. In this new conformation, the pyrrole group can give a cation- π interaction with Arg231.

Compound **23** adopts two different poses during the MD, one within pocket C and the other near pocket B, and, as for compound **10**, a cation- π interaction with Arg231 is formed for the 80% of the simulation time. Similarly, compound **35** can adopt two different poses: half of the time it

1
2
3 maintains the interaction with pocket C, while in the other half the aromatic ring bearing a nitrile
4 group is located near Phe227.
5
6
7
8
9

10 *In vitro metabolic stability*

11
12
13 The *in vitro* metabolic stability of **10**, **23** and **35** was evaluated in mouse liver microsomes (MLM)
14 activated by NADPH by measuring the substrate residual after one hour of incubation. All three
15 compounds undergo oxidative metabolism, with a residual substrate of 32%, 65% and 59%,
16 respectively. Similar percentages have been observed in the incubation mixtures supplied with
17 glutathione (GSH). Next, we performed the metabolites structural characterization by high
18 resolution mass spectrometry (HRMS), processing the raw data with a workflow aimed for drug
19 metabolites discovery provided by Compound Discoverer™ 3.0 software (Thermo Scientific™).
20 Overall, the three compounds undergo two main transformations (Figure 4): benzimidazole
21 oxidation at different positions and oxidative *N*-dealkylation at both the benzylic carbon atoms,
22 the latter leading to the formation of the corresponding carboxylic acid further reduced to aldehyde
23 and alcohol. Despite a higher metabolic stability compared to the other two analogues, the indole
24 heterocycle of **23** is susceptible to microsomal oxidation and at least three metabolites have been
25 detected. Interestingly, data analysis did not highlight the formation of GSH adducts, suggesting
26 that metabolism is not driven toward the formation of reactive species. Full data of metabolites
27 structures and mass spectral data, as well as the metabolic pathways, are given in the Supporting
28 Information.
29
30
31
32
33
34
35
36
37
38
39
40
41
42
43
44
45
46
47
48
49

50 Based on the observed liability, strategies aimed at reducing the susceptibility toward metabolism
51 might be worth of investigation. The blockage of the putative sites of hydroxylation by using
52 fluorine or deuterium atoms would presumably not impair the activity of the compounds on IDO1,
53
54
55
56
57
58
59
60

while improving resistance toward metabolism (Figure 4). While the use of fluorine is well established in medicinal chemistry, deuterium incorporation has only recently exploded,³⁶ after the approval by FDA of the first deuterated drug. Within our class of molecules, the deuterium kinetic isotope effect (DKIE) might be exploited to mitigate both the aldehyde oxidase (AO)-driven oxidation of benzimidazole ring and the amide *N*-dealkylation.³⁷

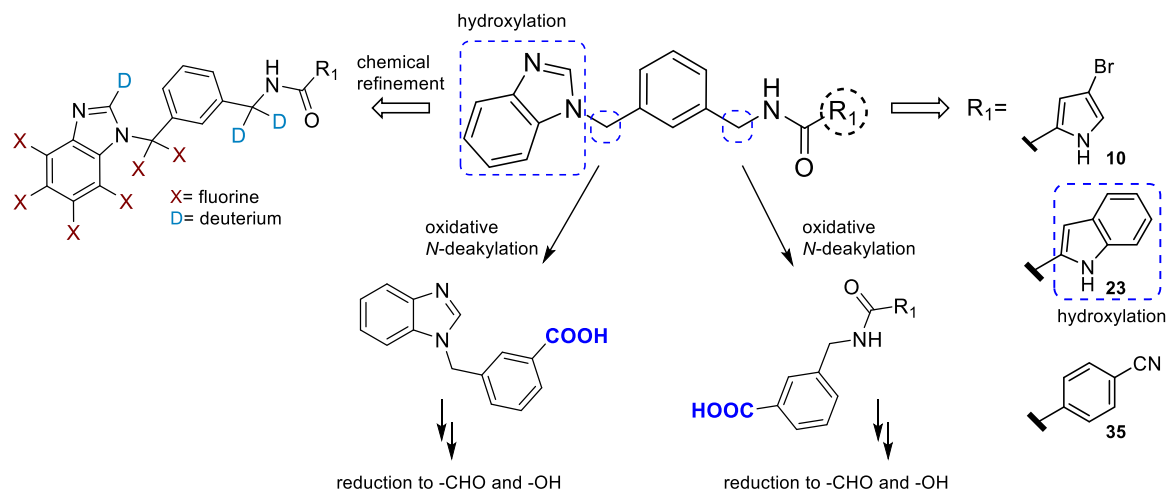


Figure 4. Metabolic pathways of compounds **10**, **23** and **35** in MLM and possible strategies to improve metabolic stability. The labile soft spots are highlighted in blue.

CYP inhibition

Since cytochrome P450 (CYP) family shares with IDO1 the iron-containing heme group, all the candidates have been evaluated for their inhibitory activity on these enzymes. Aminopyrine *N*-demethylase assay was performed in order to evaluate the inhibition of CYPs by **10**, **23** and **35** and to predict the risk of pharmacokinetic drug interactions. **10** showed a mild inhibitory activity with an IC_{50} value of 67.7 μ M compared to incubations with ketoconazole (CYP3A inhibitor), which gave an IC_{50} value of 6.4 μ M in our assay. For **23** and **35**, IC_{50} s curves could not be fitted for the absence of the bottom plateau phase which is related to their inability to inhibit CYP.

Inhibition of immunosuppressive activity of human monocytes from PDAC patients

In order to further validate the activity of our compounds, the two hits, **10** and **23**, were evaluated for their ability to inhibit the immunosuppressive activity of monocytes from patients affected by pancreatic ductal adenocarcinoma (PDAC) towards proliferation of T cells. PDAC represents the fourth leading cause of cancer death especially because of its high resistance to therapy.³⁸ PDAC cells release several pro-inflammatory molecules, thus favoring the expansion and accumulation of monocytic MDSCs that are strongly involved in promoting immune escape mechanisms exploited by cancer. We validated the immunosuppressive activity of monocytes isolated from PDAC patients (n=16). As previously shown by Trovato *et al.*,³⁹ on the basis of such immunosuppressive activity, our cohort of PDAC patients could be divided into two sub-groups: “suppressive PDAC” (n=11, red), whose monocytes were able to reduce T cell proliferation, and “non-suppressive PDAC” (n=5, blue), whose monocytes did not inhibit T cell proliferation, similarly to healthy donor (HD)-derived monocytes (n=7, black) (Figure 5A). In order to evaluate the capability of IDO1 inhibitors to reduce the immunosuppressive activity of monocytes from PDAC patients, we first selected the higher concentration that would not affect the viability of both monocytes isolated from HD (30 μ M) (Figure 5B) and PDAC patients (Figure 5C). Interestingly, the treatment of suppressive monocytes with IDO1 inhibitors **1**, **10** and **23** significantly reduced their capacity to restrict T cell proliferation (Figure 5D), suggesting the impact of IDO1 in driving the inhibitory function of PDAC-isolated suppressive monocytes. Notably, compound **10** showed a higher effect compared to epacadostat **1**. Finally, as expected, both **10** and **23** inhibitors resulted ineffective on non-suppressive PDAC-isolated monocytes (Figure 5E).

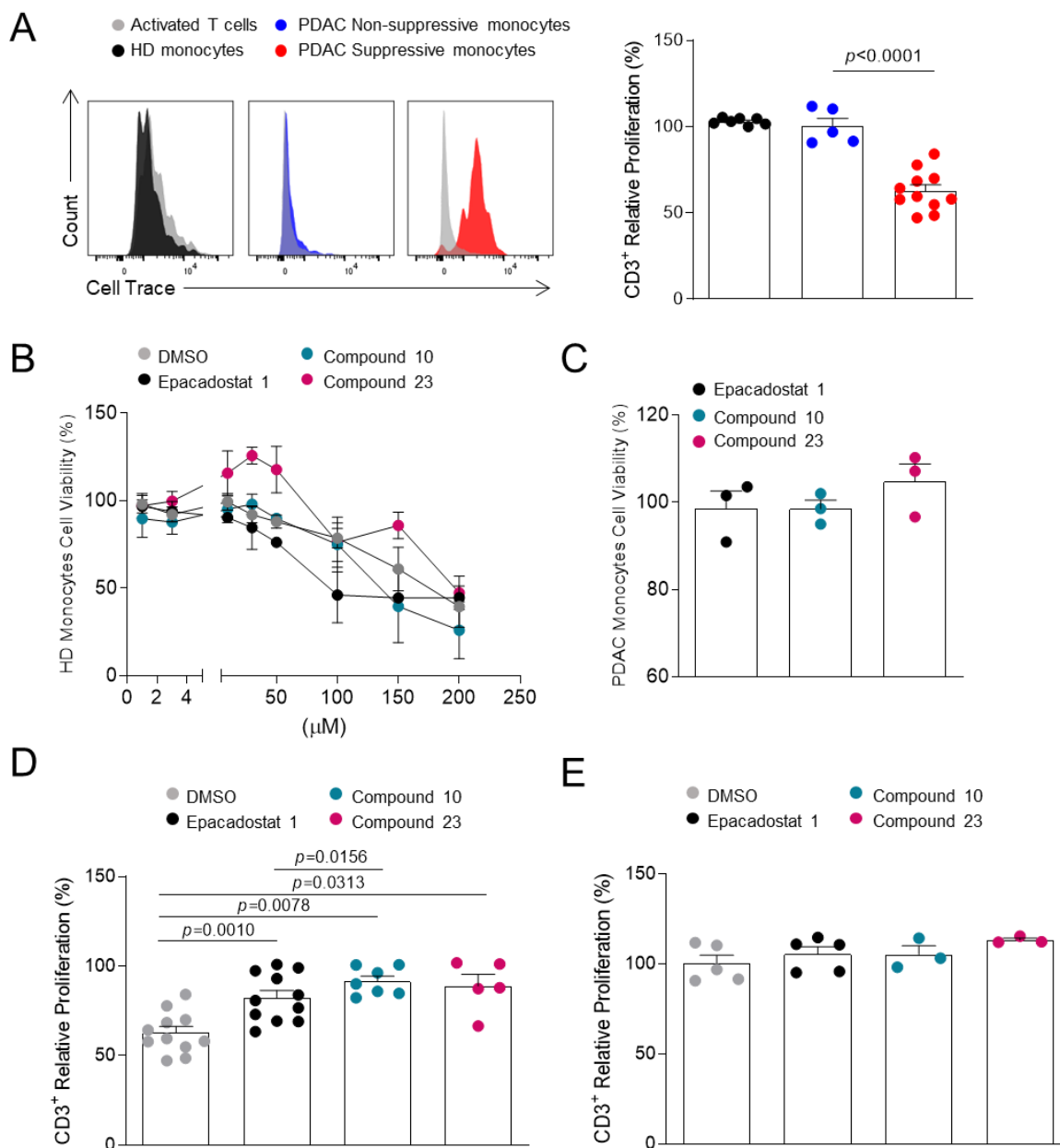


Figure 5. IDO-inhibitors abrogate immunosuppressive function of PDAC-derived monocytes. **(A)** Representative proliferation peaks of Cell Trace⁺CD3⁺ T lymphocytes following the co-culture with HD (black), PDAC non-suppressive (blue), and PDAC suppressive monocytes (red) (left panel) and relative proliferation percentage of CD3⁺T cells after the co-culture with HD (n=7, black), PDAC non-suppressive (n=5, blue), and PDAC suppressive monocytes (n=11, red) (right panel). All values are normalized on activated T cells in the absence of myeloid cells. **(B)** HD

1
2
3 monocytes (n=3) viability after a 24 h treatment with different concentrations of epacadostat **1**
4 (black), compound **10** (light blue), compound **23** (purple) and DMSO (grey) as control. All values
5 are normalized on untreated cells. (C) PDAC monocytes (n=3) viability after a 24 h treatment with
6 30 μ M of epacadostat (black), compound **10** (light blue) and compound **23** (purple). (D, E)
7 Relative proliferation percentage of CD3⁺ T cells after 4 days of co-culture with PDAC suppressive
8 (D) and PDAC non-suppressive (E) monocytes pre-treated with 30 μ M of epacadostat **1** (black),
9 compound **10** (light blue), compound **23** (purple) and DMSO (grey) as control. All values are
10 normalized on activated T cells in the absence of myeloid cells. Data are expressed as mean \pm
11 SEM. Statistical analyses were performed using Mann-Whitney test. HD: healthy donor PDAC:
12 pancreatic ductal adenocarcinoma.
13
14
15
16
17
18
19
20
21
22
23
24
25
26
27

28 ***In vivo* PK/PD of compound 23**

29
30
31 Considering the slightly higher *in vitro* metabolic stability shown by compound **23** compared to
32 **10**, we proceeded evaluating its pharmacokinetic parameters in mice. Briefly, mice were injected
33 with **23** (*i.v.* 10 mg/kg, once) and serial blood sampling was performed. **23** showed a half-life of
34 0.65 h, with a clearance of 7.5 mL/min/Kg, a volume of distribution of 6.6 L/Kg and a C_{max} of 2684
35 μ g/L (see Supporting Information for the full set of PK parameters).
36
37
38
39
40
41
42

43 At selected time points, and in particular at 0, 2, 5, 15, 30 min and 8 h after the injection of the
44 compound, the L-Kyn plasmatic levels were measured. As expected, according to the short half-
45 life of **10**, L-Kyn levels rapidly decreased up to 2 min and remained below the basal level until 30
46 min, while restoring the basal level in 8 h (see Supporting Information).
47
48
49
50
51
52
53
54
55
56
57
58
59
60

1
2
3 These data were benchmarked against epacadostat **1**, evaluating L-Kyn levels after oral
4 administration of compound **1**: a tendency in decreasing L-Kyn levels was observed, in agreement
5 with literature data.⁴⁰
6
7
8
9

10 11 12 **Discussion and Conclusions** 13

14 In this study, structure-based virtual screening was instrumental to identify a potent benzimidazole
15 compound (**10**) that is endowed with attractive features. It is a novel chemotype, not sharing
16 structural similarities with previously reported IDO1 inhibitors, and displays high synthetic
17 feasibility, together with a peculiar predicted binding mode in the active site compared to the
18 previously reported IDO1 inhibitors. The benzimidazole group is accommodated in pocket A, the
19 nitrogen of the benzimidazole ring coordinates the heme group and the long side chain protrudes
20 towards pocket C. The tight packing within the enzyme allows for an extensive bonding network,
21 including one halogen and three hydrogen bonds that contribute to a strong binding interaction
22 ($K_d = 0.36 \mu\text{M}$) and a high inhibition potency ($\text{IC}_{50} = 16 \text{ nM}$ in A375). Interestingly, MD analysis
23 reveals that this pocket is not constantly occupied as **10** flips between two poses: one where it
24 interacts with pocket C and the other where it is shifted towards pocket B, in proximity to Arg231.
25
26 The *in silico*-aided SAR study around **10** afforded a derivative, **23**, in which the bromopyrrole
27 moiety displayed by **10** is replaced by an indole group, that according to docking analysis is located
28 between pocket B and pocket C, and is able to form two hydrogen bonds with the carboxylic
29 moiety of the heme group. MD analysis highlights that **23** can flip between two different poses,
30 but simulation time spent near Arg231 is greater than compound **10**. **23** is able to inhibit IDO1 at
31 the low nanomolar level in different tumour cell lines, is not cytotoxic up to $30 \mu\text{M}$, is specific for
32 IDO1 over TDO (>1000-fold) and does not interfere with CYPs. Last, the compound can be
33
34
35
36
37
38
39
40
41
42
43
44
45
46
47
48
49
50
51
52
53
54
55
56
57
58
59
60

1
2
3 prepared through three high-yielding synthetic steps and is synthetically tractable. The *in vitro*
4 metabolic stability underlined that **23** undergoes oxidative metabolism, a liability that was further
5 confirmed by a short *in vivo* half-life. In spite of this, a significant reduction of L-Kyn levels in
6 plasma was observed when the compound was injected *i.v.* at a dose of 10 mg/kg in mice,
7 confirming the molecule as a potent IDO1 inhibitor also under *in vivo* settings. Finally, we
8 demonstrated that compound **23** has a potent effect on abrogating immunosuppressive properties
9 of MDSC-like cells isolated from PDAC patients to an extent similar to epacadostat.

10 In conclusion, a novel class of potent IDO1 inhibitors that displays a peculiar profile compared to
11 the known IDO1 inhibitors in terms of chemical structure, pose in the active site, synthetic
12 feasibility and specificity over TDO, has been discovered by a structure-based virtual screening.
13 All the accumulated data strongly suggest that these compounds might lay the basis for an
14 improvement of the effectiveness of IDO1-targeting immunotherapy. Current efforts aimed at
15 optimizing the PK profile are ongoing in our laboratory and will be reported in due course.

34 EXPERIMENTAL SECTION

37 **Molecular modelling**

38 All molecular modelling studies were performed on a Tesla workstation equipped with two Intel
39 Xeon X5650 2.67 GHz processors and with Ubuntu 14.04 (<http://www.ubuntu.com>). Protein
40 structures and 3D chemical structures were generated in PyMOL.⁴¹

46 **Compound sources**

47 The collection of compounds was retrieved from ZINC15, a searchable database that includes
48 chemical structures available from vendors.²⁹ The “in stock”-“drug-now” subset, that contains
49 molecules with drug-like properties (molecular weight <500 Da and >150, logP ≤5, number of
50 rotatable bonds ≤7, polar surface area <150, number of hydrogen bond donor ≤5 and number of
51
52
53
54
55
56
57
58
59
60

1
2
3 hydrogen bond acceptor ≤ 10), was downloaded. Using these criteria, 8.2 million structures were
4
5 retrieved. An in-house Perl script was used in order to standardize charges, enumerate ionization
6
7 states and generate tautomers at physiological pH range using QUACPAC software from
8
9 OpenEye.⁴² The latter operation was followed by a 3D structure optimization and generation of
10
11 conformers using OMEGA2 software.⁴³
12
13

14 **Virtual screening procedure**

15
16
17 In this study the X-ray structure of the 4-phenylimidazole-IDO1 complex was used (entry code
18
19 2DOT).⁴⁴ Water molecules were removed, and all the hydrogen atoms and MMFF94 charges were
20
21 added. Then, the complex was transferred into fred_receptor and prepared for docking with
22
23 FRED.³⁰ The interaction between the iron moiety of the heme group and the target molecule was
24
25 used as a constraint: if an atom of the molecule was within an acceptable distance to it, the docking
26
27 pose was retained; if not, the compound was discarded. Docked conformations were scored using
28
29 Chemgauss4.
30
31

32 **Compound 10 focused library**

33
34
35 All the available compounds bearing an acid moiety were retrieved from the ZINC database. Only
36
37 three vendors were considered (SigmaAldrich, AlfaAesar, Fluorochem) and 44,066 structures
38
39 were obtained. All the compounds were virtually combined with compound **9** using an *in-house*
40
41 python script to obtain the corresponding amides. The resulting molecules were filtered using the
42
43 virtual screening procedure already discussed in this manuscript.
44
45

46 **Molecular dynamics (MD) simulation**

47
48
49 The MD simulations were carried out using Desmond simulation package of Schrödinger LLC.³⁵
50
51 The NPT ensemble with a temperature of 300 K and a pressure of 1 bar was applied in all runs.
52
53 The simulation length was 100 ns with a relaxation time 1 ps. The OPLS_2005 force field
54
55
56
57
58
59
60

1
2
3 parameters were used in all the simulations.⁴⁵ The long-range electrostatic interactions were
4
5 calculated using the particle mesh Ewald method.⁴⁶ The cut-off radius in Coulomb interactions
6
7 was 9.0 Å. The water molecules were explicitly described using the simple point charge model.⁴⁷
8
9 The Martyna–Tuckerman–Klein chain coupling scheme⁴⁸ with a coupling constant of 2.0 ps was
10
11 used for the pressure control and the Nosé–Hoover chain coupling scheme⁴⁹ for the temperature
12
13 control. Nonbonded forces were calculated using an r-RESPA integrator where the short-range
14
15 forces were updated every step and the long-range forces were updated every three steps. The
16
17 trajectory sampling was done at an interval of 1.0 ps. The behavior and the interactions between
18
19 the ligands and protein were analyzed using the Simulation Interaction Diagram tool implemented
20
21 in Desmond MD package. The stability of MD simulations was monitored considering the RMSD
22
23 of the ligand and protein atom positions over time.
24
25
26
27

28 **Chemistry**

29
30
31 **General Experimental Methods.** Commercially available reagents and solvents were used as
32
33 purchased without further purification. When needed, solvents were distilled and stored on
34
35 molecular sieves. Column chromatography was performed on silica gel. Thin layer
36
37 chromatography (TLC) was carried out on 5 cm × 20 cm plates with a layer thickness of 0.25 mm.
38
39 When necessary, TLC plates were visualized with aqueous KMnO₄ or with aqueous Pancaldi
40
41 solution. Melting points were determined in open glass capillary with a Stuart scientific SMP3
42
43 apparatus. All the target compounds were checked by IR (FT-IR Thermo-Nicolet Avatar), ¹H-
44
45 NMR (Bruker Avance Neo 400 MHz; Jeol ECP 300 MHz), ¹³C-NMR (Bruker Avance Neo 400
46
47 MHz; Jeol ECP 300 MHz), and mass spectrometry (Thermo Finningan LCQ-deca XP-plus)
48
49 equipped with an ESI source and an ion trap detector. Chemical shifts are reported in parts per
50
51 million (ppm).
52
53
54
55
56
57
58
59
60

The purity of lead compounds was determined by high performance liquid chromatography (HPLC) using a Shimadzu HPLC system (Shimadzu, Kyoto, Japan) equipped with a *Synergi Polar* $150 \times 4.6 \text{ mm}$ ($4 \mu\text{m d.p.}$) stationary phase (Phenomenex Torrance, CA, USA) and using 0.2% formic acid in water and 0.2% formic acid in acetonitrile as eluents (for further details see Supporting Information). Purity of all lead compounds is 95% or higher.

3-((1*H*-Benzo[*d*]imidazol-1-yl)methyl)benzonitrile, (8).

To a solution of 1*H*-benzo[*d*]imidazole (3.00 g, 25.39 mmol, 1 eq) in acetone (83 mL) KOH (2.90 g, 50.79 mmol, 2 eq) and 3-(bromomethyl)benzonitrile (4.98 g, 25.39 mmol, 1 eq) were added in order. The reaction mixture was heated at 60 °C for 4 h. Then, acetone was removed in vacuo, water was added and the aqueous layer was extracted with EtOAc (x1). The organic extract was dried over Na₂SO₄, filtered and concentrated in vacuo. Purification by silica gel column chromatography using PE/EtOAc 3:7 provided the desired compound (5.86 g, 25.14 mmol, 99%) as a yellow solid. Mp 110-112 °C. ¹H-NMR (300 MHz, CDCl₃): δ = 7.98 (s, 1H), 7.83 (d, *J* = 7.7 Hz, 1H), 7.59 (d, *J* = 7.7 Hz, 1H), 7.76 (s, 1H), 7.43 (d, *J* = 7.4 Hz, 1H), 7.33-7.25 (m, 3H), 7.22 (t, *J* = 7.4 Hz, 1H), 5.40 (s, 2H). ¹³C-NMR (75 MHz, CD₃OD): δ = 143.9, 143.3, 137.4, 133.6, 131.9, 131.4, 130.4, 130.0, 123.6, 122.7, 120.5, 118.4, 113.0, 110.0, 47.9. IR (KBr): $\tilde{\nu}$ = 3099, 3077, 3051, 2865, 2757, 2560, 1496, 1439, 743 cm⁻¹. MS (ESI): *m/z* 234 [M + H]⁺.

(3-((1*H*-Benzo[*d*]imidazol-1-yl)methyl)phenyl)methanamine, (9).

Compound **8** (1.50 g, 6.43 mmol, 1 eq) was solubilized in dry THF (49 mL). The solution was cooled to 0 °C and LiAlH₄ (0.49 g, 16.09 mmol, 2.5 eq) was slowly added. The mixture was stirred at rt overnight and then heated at 65 °C for 2 h. Then, the reaction was quenched with EtOAc and with saturated aqueous solution of Na₂SO₄. The mixture was filtered over a pad of celite and rinsed with EtOAc. Purification by silica gel column chromatography using EtOAc /MeOH 7:3 as eluent

provided the title compound (1.07 g, 4.50 mmol, 70%) as a yellow oil. ¹H-NMR (300 MHz, CD₃OD): δ = 8.28 (s, 1H), 7.66 (t, *J* = 7.2 Hz, 1H), 7.43 (t, *J* = 7.2 Hz, 1H), 7.30-7.15 (m, 6H), 5.74 (s, 2H), 3.75 (s, 2H). ¹³C-NMR (75 MHz, CD₃OD): δ = 143.9, 143.2, 137.4, 133.6, 131.9, 131.4, 130.4, 130.0, 123.6, 122.7, 120.5, 118.4, 113.0, 110.0, 47.8. IR (KBr): $\tilde{\nu}$ = 3359, 3048, 2984, 1730, 1494, 1438, 1286, 1201, 741 cm⁻¹. MS (ESI): *m/z* 238 [M + H]⁺.

General procedure for the synthesis of compounds **10**, **14**, **18-39**, **53**.

To a solution of compound **9** (167.11 mg, 0.7 mmol, 1 eq) in dry CH₂Cl₂ (5 mL) TEA (220 μL, 1.54 mmol, 2.2 eq), EDCI (161.28 mg, 0.84 mmol, 1.2 eq), HOBT (113.51 mg, 0.84 mmol, 1.2 eq) and carboxylic acid (0.84 mmol, 1.2 eq) were added in order. The resulting mixture was stirred at room temperature for 16 h. CH₂Cl₂ was added and the organic phase was washed with aqueous saturated NH₄Cl solution (x1), dried over Na₂SO₄ and evaporated. Purification by silica gel column chromatography afforded compounds **10**, **14**, **18-39**, **53**.

N-(3-((1*H*-Benzo[*d*]imidazol-1-yl)methyl)benzyl)-4-bromo-1*H*-pyrrole-2-carboxamide, (**10**).

The title compound was synthesized following the general procedure, starting from compound **9** (90 mg, 0.38 mmol) and 4-bromo-1*H*-pyrrole-2-carboxylic acid (86 mg, 0.46 mmol). The crude material was purified by column chromatography using PE/EtOAc 2:8 as eluent to afford compound **10** (77 mg, 0.19 mmol, 50%) as a white solid. Mp 212-214 °C. ¹H-NMR (400 MHz, CD₃OD): δ = 8.21 (s, 1H), 7.65 (d, *J* = 7.4 Hz, 1H), 7.38 (d, *J* = 7.6 Hz, 1H), 7.31-7.12 (m, 6H), 6.90 (s, 1H), 6.73 (s, 1H), 5.44 (s, 2H), 4.44 (s, 2H). ¹³C-NMR (100.6 MHz, DMSO-*d*₆): δ = 160.1, 144.6, 144.1, 140.8, 137.5, 134.1, 129.2, 127.2, 127.1, 126.8, 126.4, 122.8, 122.0, 121.8, 119.9, 112.1, 111.2, 95.5, 48.1, 42.3. IR (KBr): $\tilde{\nu}$ = 3285, 3118, 2913, 2850, 2446, 2360, 3242, 1945, 1722, 748 cm⁻¹. MS (ESI): *m/z* 409 [M + H]⁺.

3-((1*H*-Indol-1-yl)methyl)benzotrile, (**12**).

To a solution of 1*H*-indole **11** (300 mg, 2.56 mmol, 1 eq) in acetone (6 mL) KOH (287 mg, 5.12 mmol, 2 eq) and 3-(bromomethyl)benzotrile (502 mg, 2.56 mmol, 1 eq) were added in order. The reaction mixture was heated at 60 °C for 4 h. Then, acetone was removed in vacuo, water was added and the aqueous layer was extracted with EtOAc (x3). The organic extract was dried over Na₂SO₄, filtered and concentrated in vacuo. Purification by silica gel column chromatography using PE/EtOAc 9:1 provided the desired compound (425 mg, 1.83 mmol, 71%) as a yellow oil. ¹H-NMR (400 MHz, CDCl₃): δ = 7.79 (d, *J* = 7.5 Hz, 1H), 7.53 (d, *J* = 7.5 Hz, 1H), 7.40 (s, 1H), 7.35 (t, *J* = 7.5 Hz, 1H), 7.30-7.26 (m, 4H), 7.18 (d, *J* = 3.2 Hz, 1H), 6.71 (d, *J* = 3.2 Hz, 1H), 5.30 (s, 2H). ¹³C-NMR (100.6 MHz, CDCl₃): δ = 139.7, 136.2, 135.8, 134.8, 130.1, 129.8, 128.2, 126.7, 123.6, 122.7, 120.5, 119.6, 118.3, 112.9, 100.9, 51.9. IR (neat): $\tilde{\nu}$ = 3053, 2918, 2228, 1483, 1461, 1314, 471, 685 cm⁻¹. MS (ESI): *m/z* 233 [M + H]⁺.

(3-((1*H*-Indol-1-yl)methyl)phenyl)methanamine, (13).

Compound **12** (416 mg, 1.79 mmol, 1 eq) was solubilized in dry THF (6 mL). The solution was cooled to 0 °C and LiAlH₄ (170 mg, 4.48 mmol, 2.5 eq) was slowly added. The mixture was heated at 65 °C for 7 h and then was stirred at rt overnight. The reaction was quenched with EtOAc and then with saturated aqueous solution of Na₂SO₄. The mixture was filtered over a pad of celite and rinsed with EtOAc. Purification by silica gel column chromatography using EtOAc/MeOH 7:3 as eluent provided the title compound (194 mg, 0.82 mmol, 46%) as a colorless oil. ¹H-NMR (400 MHz, CDCl₃): δ = 7.76 (d, *J* = 7.8 Hz, 1H), 7.38 (d, *J* = 7.8 Hz, 1H), 7.37-7.19 (m, 6H), 7.05 (d, *J* = 6.8 Hz, 1H), 6.66 (s, 1H), 5.33 (s, 2H), 3.83 (s, 2H). ¹³C-NMR (100.6 MHz, CDCl₃): δ = 138.1, 136.3, 129.2, 129.1, 128.8, 128.2, 127.7, 126.8, 125.8, 121.7, 121.0, 119.6, 109.7, 101.7, 64.7, 50.0. IR (neat): $\tilde{\nu}$ = 3049, 2917, 2852, 1461, 1313, 735, 693 cm⁻¹. MS (ESI): *m/z* 237 [M + H]⁺.

***N*-3-((1*H*-Indol-1-yl)methyl)benzyl)-4-bromo-1*H*-pyrrole-2-carboxamide, (14).**

The title compound was synthesized following the general procedure, starting from compound **13** (186 mg, 0.79 mmol) and 4-bromo-1*H*-pyrrole-2-carboxylic acid (179 mg, 0.94 mmol). The crude material was purified by column chromatography using PE/EtOAc 5:5 as eluent to afford compound **14** (178 mg, 0.43 mmol, 54%) as a white solid. Mp 80-81 °C. ¹H-NMR (400 MHz, CDCl₃): δ = 9.89 (br s, 1H), 7.67 (d, *J* = 7.2 Hz, 1H), 7.28-7.26 (m, 2H), 7.23 (s, 1H), 7.15-7.13 (m, 3H), 7.06-7.04 (m, 2H), 6.87 (s, 1H), 6.56 (d, *J* = 3.1 Hz, 1H), 6.49 (s, 1H), 6.11 (br s, 1H), 5.33 (s, 2H), 4.52 (d, *J* = 5.8 Hz, 2H). IR (neat): $\tilde{\nu}$ = 3052, 2919, 2854, 1623, 1557, 1509, 1314, 919, 738 cm⁻¹. MS (ESI): *m/z* 409 [M + H]⁺.

(3-((1*H*-Benzo[*d*]imidazol-1-yl)methyl)phenyl)methanol, (16).

To a solution of 1*H*-benzo[*d*]imidazole (118 mg, 1.00 mmol, 1 eq) in acetone (4 mL) KOH (112 mg, 2.00 mmol, 2 eq) and (3-(bromomethyl)phenyl)methanol **15** (201 mg, 1.00 mmol, 1 eq) were added in order. The reaction mixture was heated at 60 °C for 2 h. Then, acetone was removed in vacuo, water was added and the aqueous layer was extracted with EtOAc (x3). The organic extract was dried over Na₂SO₄, filtered and concentrated in vacuo. Purification by silica gel column chromatography using EtOAc/MeOH 9:1 provided the desired compound (81 mg, 0.34 mmol, 34%) as a yellow oil. ¹H-NMR (400 MHz, CDCl₃): δ = 7.85 (s, 1H), 7.73 (d, *J* = 6.8 Hz, 1H), 7.29-7.28 (m, 3H), 7.26-7.23 (m, 3H), 7.06 (d, *J* = 6.4 Hz, 1H), 5.26 (s, 2H), 4.67 (s, 2H). ¹³C-NMR (100.6 MHz, CDCl₃): δ = 143.0, 142.6, 135.4, 133.7, 129.1, 126.8, 126.1, 125.6 (2C), 123.3, 122.6, 119.9, 110.2, 64.2, 48.9. IR (neat): $\tilde{\nu}$ = 3093, 2922, 2853, 1733, 1492, 735, 691 cm⁻¹. MS (ESI): *m/z* 239 [M + H]⁺.

3-((1*H*-Benzo[*d*]imidazol-1-yl)methyl)benzyl 4-bromo-1*H*-pyrrole-2-carboxylate, (17).

To a solution of compound **16** (70 mg, 0.29 mmol, 1 eq) in dry CH₂Cl₂ (2 mL) TEA (45 μL, 0.32 mmol, 1.1 eq), EDCI (61.3 mg, 0.32 mmol, 1.1 eq), DMAP (3.5 mg, 0.029 mmol, 0.1 eq) and 4-

1
2
3 bromo-1*H*-pyrrole-2-carboxylic acid (55 mg, 0.29 mmol, 1 eq) were added in order. The resulting
4
5 mixture was stirred at room temperature for 18 h. Then, CH₂Cl₂ was added and the organic phase
6
7 was washed with water (x1), dried over Na₂SO₄ and evaporated. Purification by silica gel column
8
9 chromatography using PE/EtOAc 2:8 provided the desired compound (48 mg, 0.12 mmol, 40%)
10
11 as a white solid. Mp 171-172 °C. ¹H-NMR (400 MHz, CD₃OD): δ = 8.29 (s, 1H), 7.69 (d, *J* = 7.0
12
13 Hz, 1H), 7.43 (d, *J* = 6.9 Hz, 1H), 7.39-7.35 (m, 3H), 7.28-7.23 (m, 3H), 6.98 (d, *J* = 1.56 Hz,
14
15 1H), 6.78 (d, *J* = 1.56 Hz, 1H), 5.54 (s, 2H), 5.27 (s, 2H). IR (neat): $\tilde{\nu}$ = 2922, 2851, 1701, 1398,
16
17 1186, 1135, 775, 741 cm⁻¹. MS (ESI): *m/z* 411 [M + H]⁺.

18
19
20
21 ***N*-(3-((1*H*-Benzo[*d*]imidazol-1-yl)methyl)benzyl)-1*H*-pyrrole-2-carboxamide, (18).**

22
23 The title compound was synthesized following the general procedure, starting from compound **9**
24
25 (166 mg, 0.70 mmol) and 1*H*-pyrrole-2-carboxylic acid (93 mg, 0.84 mmol). The crude material
26
27 was purified by column chromatography using PE/EtOAc 2:8 as eluent to afford compound **18**
28
29 (143 mg, 0.43 mmol, 62%) as a yellow solid. Mp 206-208 °C. ¹H-NMR (300 MHz, CD₃OD): δ =
30
31 8.23 (s, 1H), 7.64 (dd, *J*_s = 1.0, 8.3 Hz), 7.39 (d, *J* = 6.9 Hz, 1H), 7.26-7.13 (m, 7H), 7.76 (s, 1H),
32
33 6.16 (d, *J* = 2.5 Hz, 1H), 5.43 (s 2H), 5.36 (s, 2H). IR (KBr): $\tilde{\nu}$ = 3220, 3087, 2935, 2701, 2563,
34
35 1628, 1560, 1491, 1437, 1438, 776, 745 cm⁻¹. MS (ESI): *m/z* 331 [M + H]⁺.

36
37
38
39 ***N*-(3-((1*H*-Benzo[*d*]imidazol-1-yl)methyl)benzyl)furan-2-carboxamide, (19).**

40
41 The title compound was synthesized following the general procedure, starting from compound **9**
42
43 (166 mg, 0.70 mmol) and furan-2-carboxylic acid (94 mg, 0.84 mmol). The crude material was
44
45 purified by column chromatography using PE/EtOAc 4:6 as eluent to afford compound **19** (150
46
47 mg, 0.46 mmol, 65%) as a white solid. Mp 153-154 °C. ¹H-NMR (300 MHz, CD₃OD): δ = 8.19
48
49 (s, 1H), 7.64-7.57 (m, 3H), 7.34 (d, *J* = 7.4 Hz, 1H), 7.35-7.04 (m, 7H), 5.36 (s, 2H), 4.44 (s, 2H).
50
51
52
53
54
55
56
57
58
59
60

1
2
3 IR (KBr): $\tilde{\nu}$ = 3477, 3231, 3070, 2977, 2926, 1742, 1638, 1495, 1442, 1365, 1015, 769, 745 cm^{-1} .

4
5 MS (ESI): m/z 332 [M + H]⁺.

6
7
8 ***N*-(3-((1*H*-Benzo[*d*]imidazol-1-yl)methyl)benzyl)thiophene-2-carboxamide, (20).**

9
10 The title compound was synthesized following the general procedure, starting from compound **9**
11 (160 mg, 0.67 mmol) and thiophene-2-carboxylic acid (103 mg, 0.81 mmol). The crude material
12 was purified by column chromatography using PE/EtOAc 3:7 as eluent to afford compound **20**
13 (182 mg, 0.52 mmol, 78%) as a yellow solid. Mp 171-173 °C. ¹H-NMR (300 MHz, CD₃OD): δ =
14 8.19 (s, 1H), 7.64-7.57 (m, 3H), 7.34 (d, J = 7.4 Hz, 1H), 7.35-7.04 (m, 7H), 5.36 (s, 2H), 4.44 (s,
15 2H). IR (KBr): $\tilde{\nu}$ = 3555, 3414, 3263, 3070, 2892, 1636, 1618, 1498, 1365, 744 cm^{-1} . MS (ESI):
16 m/z 348 [M + H]⁺.

17
18
19
20
21
22
23
24
25
26 ***N*-(3-((1*H*-Benzo[*d*]imidazol-1-yl)methyl)benzyl)benzofuran-2-carboxamide, (21).**

27
28 The title compound was synthesized following the general procedure, starting from compound **9**
29 (166 mg, 0.70 mmol) and benzofuran-2-carboxylic acid (136 mg, 0.84 mmol). The crude material
30 was purified by column chromatography using PE/EtOAc 3:7 as eluent to afford compound **21** (98
31 mg, 0.26 mmol, 37%) as a yellow solid. Mp 161-163 °C. ¹H-NMR (300 MHz, CD₃OD): δ = 8.26
32 (s, 1H), 7.65 (d, J = 7.9 Hz, 1H), 7.60-7.57 (s, 1H), 7.50 (d, J = 7.9 Hz, 1H), 7.41 (m, 2H), 7.36-
33 7.31 (m, 2H), 7.25 (m, 3H), 7.13-7.10 (m, 3H), 5.43 (s, 2H), 4.52 (s, 2H). ¹³C-NMR (100.6 MHz,
34 DMSO-*d*₆): δ = 158.6, 154.7, 149.5, 140.3 (2C), 137.5 (2C), 133.9, 129.2, 127.6, 127.3, 127.3,
35 126.9, 126.5, 124.2, 123.2, 122.8, 122.1, 119.9, 112.3, 111.2, 110.0, 48.1, 42.5. IR (KBr): $\tilde{\nu}$ =
36 3892, 3801, 3735, 2927, 2850, 1734, 1590, 1560, 1496, 1474, 747 cm^{-1} . MS (ESI): 382 m/z [M +
37 H]⁺.

38
39
40
41
42
43
44
45
46
47
48
49
50
51 ***N*-(3-((1*H*-Benzo[*d*]imidazol-1-yl)methyl)benzyl)benzo[*b*]thiophene-2-carboxamide, (22).**

1
2
3 The title compound was synthesized following the general procedure, starting from compound **9**
4 (166 mg, 0.70 mmol) and benzo[*b*]thiophene-2-carboxylic acid (149 mg, 0.84 mmol). The crude
5 material was purified by column chromatography using PE/EtOAc 5:5 as eluent to afford
6 compound **22** (144 mg, 0.36 mmol, 52%) as a white solid. Mp 185-187 °C. ¹H-NMR (300 MHz,
7 acetone-*d*₆): δ = 8.48 (s, 1H), 8.23 (s, 1H), 8.00-7.98 (m, 2H), 7.89 (dd, *J*_S = 1.9, 7.1 Hz, 1H), 7.77-
8 7.63 (m, 1H), 7.48-7.47 (m, 2H), 7.44-7.41 (m, 2H), 7.33-7.28 (d, *J* = 5.8 Hz, 2H), 7.21-7.11 (m,
9 2H), 5.50 (s, 2H), 4.59 (s, 2H). IR (KBr): $\tilde{\nu}$ = 3183, 3055, 1642, 1560, 1495, 1458, 1290, 742 cm⁻¹.
10
11
12
13
14
15
16
17
18
19 ¹. MS (ESI): *m/z* 398 [M + H]⁺.

20
21
22 ***N*-(3-((1*H*-Benzo[*d*]imidazol-1-yl)methyl)benzyl)-1*H*-indole-2-carboxamide, (23).**

23
24 The title compound was synthesized following the general procedure, starting from compound **9**
25 (166 mg, 0.70 mmol) and 1*H*-indole-2-carboxylic acid (135 mg, 0.84 mmol). The crude material
26 was purified by column chromatography using PE/EtOAc 4:6 as eluent to afford compound **23**
27 (144 mg, 0.38 mmol, 54%) as a yellow solid. Mp 231-233 °C. ¹H-NMR (400 MHz, DMSO-*d*₆): δ
28 = 11.53 (br s, 1H), 8.94 (br s, 1H), 8.37 (s, 1H), 7.68-7.55 (m, 2H), 7.53-7.40 (m, 2H), 7.37 (s,
29 1H), 7.31-7.26 (m, 2H), 7.21-7.15, (m, 5H), 7.04 (t, *J* = 7.9 Hz, 1H), 5.49 (s, 2H), 4.48 (s, 2H).
30
31
32
33
34
35
36
37
38 ¹³C-NMR (100.6 MHz, DMSO-*d*₆): δ = 161.6, 144.7, 144.1, 140.7, 137.5, 136.9, 134.2, 132.0,
39 129.2, 127.6, 127.2, 126.9, 126.4, 123.8, 122.8, 122.0, 121.9, 120.2, 119.9, 112.8, 111.2, 103.1,
40 48.1, 42.5. IR (KBr): $\tilde{\nu}$ = 3218, 3053, 2926, 2853, 2721, 2648, 1638, 1564, 1495, 1310, 746 cm⁻¹.
41
42
43
44
45 MS (ESI): *m/z* 381 [M + H]⁺.

46
47 ***N*-(3-((1*H*-Benzo[*d*]imidazol-1-yl)methyl)benzyl)-5-methyl-1*H*-indole-2-carboxamide, (24).**

48
49 The title compound was synthesized following the general procedure, starting from compound **9**
50 (166 mg, 0.70 mmol) and 5-methyl-1*H*-indole-2-carboxylic acid (147 mg, 0.84 mmol). The crude
51 material was purified by column chromatography using PE/EtOAc 3:7 as eluent to afford
52
53
54
55
56
57
58
59
60

1
2
3 compound **24** (134 mg, 0.34 mmol, 49%) as a white solid. Mp 222-224 °C. ¹H-NMR (300 MHz,
4 CD₃OD): δ = 8.25 (s, 1H), 7.62 (dd, *J*_S = 1.9, 7.7 Hz, 1H), 7.41-7.28 (m, 6H), 7.18-7.16 (m, 3H),
5 7.61 (d, *J* = 7.7 Hz, 1H), 6.93 (s, 1H), 5.48 (s, 2H), 4.53 (s, 2H), 2.40 (s, 3H). ¹³C-NMR (100.6
6 MHz, DMSO-*d*₆): δ = 161.7, 144.7, 144.0, 140.8, 137.5, 135.4, 134.1, 132.0, 129.2, 128.7, 127.8,
7 127.2, 126.9, 126.4, 125.6, 122.8, 122.0, 121.2, 119.9, 112.5, 111.2, 102.6, 48.1, 42.5, 21.6. IR
8 (KBr): $\tilde{\nu}$ = 3232, 3090, 3061, 2922, 1637, 1560, 1496, 1419, 802, 736 cm⁻¹. MS (ESI): *m/z* 395 [M
9 + H]⁺.

10
11
12
13
14
15
16
17
18
19 ***N*-(3-((1*H*-Benzo[*d*]imidazol-1-yl)methyl)benzyl)-5-hydroxy-1*H*-indole-2-carboxamide, (25).**

20
21 The title compound was synthesized following the general procedure, starting from compound **9**
22 (166 mg, 0.70 mmol) and 5-hydroxy-1*H*-indole-2-carboxylic acid (148 mg, 0.84 mmol). The crude
23 material was purified by column chromatography using PE/EtOAc 3:7 as eluent to afford
24 compound **25** (35 mg, 0.09 mmol, 13%) as a yellow solid. Mp 210-212 °C. ¹H-NMR (300 MHz,
25 acetone-*d*₆): δ = 10.42 (br s, 1H), 8.32 (s, 1H), 7.52(dd, *J*_S = 1.7, 7.1 Hz, 1H), 7.32-7.20 (m, 6H),
26 7.18-7.15 (m, 3H), 7.59 (d, *J* = 7.7 Hz, 1H), 7.01 (s, 1H), 5.67 (br s, 1H), 5.50 (s, 2H), 4.58 (s,
27 2H), 3.31 (br s, 1H). IR (KBr): $\tilde{\nu}$ = 3745, 2359, 2342, 1742, 1557, 1496, 1362, 1257 cm⁻¹. MS
28 (ESI): *m/z* 397 [M + H]⁺.

29
30
31
32
33
34
35
36
37
38
39
40 ***N*-(3-((1*H*-Benzo[*d*]imidazol-1-yl)methyl)benzyl)-5-methoxy-1*H*-indole-2-carboxamide,**
41
42 **(26).**

43
44 The title compound was synthesized following the general procedure, starting from compound **9**
45 (166 mg, 0.70 mmol) and 5-methoxy-1*H*-indole-2-carboxylic acid (160 mg, 0.84 mmol). The
46 crude material was purified by column chromatography using PE/EtOAc 2:8 as eluent to afford
47 compound **26** (160 mg, 0.39 mmol, 56%) as a yellow solid. Mp 225-227 °C. ¹H-NMR (300 MHz,
48 DMSO-*d*₆): δ = 11.43 (br s, 1H), 8.97 (s, 1H), 8.39 (s, 1H), 7.65 (d, *J* = 7.1 Hz, 1H), 7.50 (d, *J* =
49
50
51
52
53
54
55
56
57
58
59
60

1
2
3 7.1 Hz, 1H), 7.33 (t, $J = 6.3$ Hz, 1H), 7.27 (d, $J = 6.3$ Hz, 2H), 7.22-7.18 (m, 3H), 7.06 (d, $J = 6.3$
4 Hz, 2H), 6.83 (d, $J = 8.5$ Hz, 1H), 5.48 (s, 2H), 4.47 (s, 2H), 3.75 (s, 3H). IR (KBr): $\tilde{\nu} = 3246,$
5
6 3087, 3004, 2926, 2803, 1637, 1559, 1497, 1359, 1269, 163, 742 cm^{-1} . MS (ESI): 411 m/z [$M +$
7
8 H]⁺.
9

10
11
12 ***N*-(3-((1*H*-Benzo[*d*]imidazol-1-yl)methyl)benzyl)-1*H*-benzo[*d*]imidazole-2-carboxamide,**
13
14
15 **(27).**
16

17 The title compound was synthesized following the general procedure, starting from compound **9**
18 (166 mg, 0.70 mmol) and 1*H*-benzo[*d*]imidazole-2-carboxylic acid (136 mg, 0.84 mmol). The
19 crude material was purified by column chromatography using PE/EtOAc 4:6 as eluent to afford
20 compound **27** (229 mg, 0.60 mmol, 86%) as a white solid. Mp 226-227 °C. ¹H-NMR (300 MHz,
21 DMSO-*d*₆): $\delta = 9.40$ (br s, 1H), 8.34 (s, 1H), 7.77-7.58 (m, 3H), 7.47 (d, $J = 7.2$ Hz, 1H), 7.36 (s,
22 1H), 7.27-7.21 (m, 4H), 7.16-7.06 (m, 3H), 5.46 (s, 2H), 4.46 (s, 2H). ¹³C-NMR (100.6 MHz,
23 DMSO-*d*₆): $\delta = 159.5, 146.2, 144.7$ (2C), 144.2, 140.4, 137.5, 134.3, 129.3, 127.4 (2C), 127.1
24 (2C), 126.5, 123.9, 122.9, 122.3, 122.1, 120.0 (2C), 111.2, 48.3, 42.8. IR (KBr): $\tilde{\nu} = 3418, 3047,$
25
26 1666, 1507, 1494, 1436, 1330, 744 cm^{-1} . MS (ESI): m/z 382 [$M + H$]⁺.
27
28
29
30
31
32
33
34
35
36
37

38 ***N*-(3-((1*H*-Benzo[*d*]imidazol-1-yl)methyl)benzyl)-2-(benzo[*d*][1,3]dioxol-5-yl)acetamide,**
39
40
41 **(28).**
42

43 The title compound was synthesized following the general procedure, starting from compound **9**
44 (166 mg, 0.70 mmol) and 2-(benzo[*d*][1,3]dioxol-5-yl)acetic acid (151 mg, 0.84 mmol). The crude
45 material was purified by column chromatography using PE/EtOAc 3:7 as eluent to afford
46 compound **28** (235 mg, 0.59 mmol, 84%) as an amorphous yellow solid. ¹H-NMR (300 MHz,
47 CD₃OD): $\delta = 8.13$ (s, 1H), 7.66 (d, $J = 8.0$ Hz, 1H), 7.29 (d, $J = 8.0$ Hz, 1H), 7.30-7.00 (m, 7H),
48
49 6.74 (s, 1H), 6.66 (s, 1H), 5.76 (s, 2H), 5.27 (s, 2H), 4.23 (s, 2H), 3.30 (s, 2H). IR (KBr): $\tilde{\nu} = 3735,$
50
51
52
53
54
55
56
57
58
59
60

3629, 3255, 2887, 2790, 1845, 1654, 1500, 1442, 1260, 1190, 1040, 668 cm⁻¹. MS (ESI): *m/z* 400 [M + H]⁺.

***N*-(3-((1*H*-Benzo[*d*]imidazol-1-yl)methyl)benzyl)benzamide, (29).**

The title compound was synthesized following the general procedure, starting from compound **9** (166 mg, 0.70 mmol) and benzoic acid (102 mg, 0.84 mmol). The crude material was purified by column chromatography using PE/EtOAc 3:7 as eluent to afford compound **29** (128 mg, 0.39 mmol, 54%) as a white solid. ¹H-NMR (300 MHz, CD₃OD): δ = 8.24 (s, 1H), 7.75 (d, *J* = 8.2 Hz, 2H), 7.64 (d, *J* = 8.2 Hz, 1H), 7.55-7.49 (m, 1H), 7.43 (t, *J* = 7.7 Hz, 1H), 7.38 (d, *J* = 7.7 Hz, 1H), 7.31-7.15 (m, 7H), 5.45 (s, 2H), 4.51 (s, 2H). MS (ESI): *m/z* 342 [M + H]⁺.

***N*-(3-((1*H*-Benzo[*d*]imidazol-1-yl)methyl)benzyl)-4-methylbenzamide, (30).**

The title compound was synthesized following the general procedure, starting from compound **9** (76 mg, 0.32 mmol) and 2-oxo-2-(*p*-tolyl)acetic acid (52 mg, 0.38 mmol). The crude material was purified by column chromatography using PE/EtOAc 3:7 as eluent to afford compound **30** (79 mg, 0.21 mmol, 69%) as a white solid. Mp 137-139 °C. ¹H-NMR (300 MHz, CD₃OD): δ = 8.22 (s, 1H), 7.81-7.58 (m, 3H), 7.38 (d, *J* = 7.6 Hz, 1H), 7.36-7.06 (m, 8H), 5.43 (s, 2H), 4.90 (s, 2H), 2.36 (s, 3H). ¹³C-NMR (100.6 MHz, DMSO-*d*₆): δ = 166.6, 144.7, 144.0, 141.5, 140.9, 137.4, 134.1, 132.0, 129.3 (2C), 129.2, 127.7 (2C), 127.1, 126.8, 126.3, 122.8, 122.0, 119.9, 111.2, 48.1, 42.9, 21.4. MS (ESI): 356 *m/z* [M + H]⁺.

***N*-(3-((1*H*-Benzo[*d*]imidazol-1-yl)methyl)benzyl)-4-(trifluoromethyl)benzamide, (31).**

The title compound was synthesized following the general procedure, starting from compound **9** (60 mg, 0.25 mmol) and 4-(trifluoromethyl)benzoic acid (57 mg, 0.30 mmol). The crude material was purified by column chromatography using PE/EtOAc 3:7 as eluent to afford compound **31** (84 mg, 0.21 mmol, 82%) as a white solid. Mp 154-156 °C. ¹H-NMR (300 MHz, CD₃OD): δ = 8.27

(s, 1H), 7.89 (d, $J = 8.2$ Hz, 2H), 7.75 (d, $J = 8.2$ Hz, 2H), 7.64 (d, $J = 7.4$ Hz, 1H), 7.39 (d, $J = 8.2$ Hz, 1H), 7.33-7.12 (m, 6H), 5.49 (s, 2H), 4.52 (s, 2H). ^{13}C -NMR (100.6 MHz, $\text{DMSO-}d_6$): $\delta = 165.6, 144.7, 144.0, 141.3$ (q, $J = 441.6$ Hz), 140.4 (2C), 137.5 (2C), 131.6 (q, $J = 32.2$ Hz), 129.2, 128.6, 127.1, 126.7, 126.5, 125.8 (q, $J = 4.0$ Hz), 122.8, 122.0, 119.9, 111.1, 48.1, 43.0. MS (ESI): 410 m/z $[\text{M} + \text{H}]^+$.

***N*-(3-((1*H*-Benzo[*d*]imidazol-1-yl)methyl)benzyl)-4-bromobenzamide, (32).**

The title compound was synthesized following the general procedure, starting from compound **9** (60 mg, 0.25 mmol) and 4-bromobenzoic acid (61 mg, 0.30 mmol). The crude material was purified by column chromatography using PE/EtOAc 3:7 as eluent to afford compound **32** (81 mg, 0.19 mmol, 77%) as a white solid. Mp 151-153 °C. ^1H -NMR (300 MHz, CD_3OD): $\delta = 8.27$ (s, 1H), 7.73-7.56 (m, 5H), 7.41 (d, $J = 7.1$ Hz, 1H), 7.35 (d, $J = 7.4$ Hz, 2H), 7.29-7.18 (m, 4H), 5.50 (s, 2H), 4.61 (s, 2H). ^{13}C -NMR (100.6 MHz, $\text{DMSO-}d_6$): $\delta = 165.8, 144.7, 144.0, 140.5, 137.5, 134.1, 133.9, 131.8, 129.9, 129.2, 127.1, 126.7, 126.4, 125.4, 122.8, 122.0, 119.9, 111.2, 48.1, 42.9$. MS (ESI): 420 m/z $[\text{M} + \text{H}]^+$.

***N*-(3-((1*H*-Benzo[*d*]imidazol-1-yl)methyl)benzyl)-4-chlorobenzamide, (33).**

The title compound was synthesized following the general procedure, starting from compound **9** (60 mg, 0.25 mmol) and 4-chlorobenzoic acid (47 mg, 0.30 mmol). The crude material was purified by column chromatography using PE/EtOAc 3:7 as eluent to afford compound **33** (57 mg, 0.15 mmol, 60%) as a white solid. Mp 125-127 °C. ^1H -NMR (300 MHz, CD_3OD): $\delta = 8.25$ (s, 1H), 7.73 (d, $J = 8.5$ Hz, 2H), 7.65 (d, $J = 7.1$ Hz, 1H), 7.49-7.37 (m, 3H), 7.33-7.09 (m, 6H), 5.48 (s, 2H), 4.50 (s, 2H). ^{13}C -NMR (100.6 MHz, $\text{DMSO-}d_6$): $\delta = 165.7, 144.7, 144.0, 140.6, 137.5, 136.5, 134.1, 133.5, 129.7, 129.2, 128.9, 127.1, 126.7, 126.4, 122.8, 122.0, 119.9, 111.2, 48.1, 42.9$. MS (ESI): 376 m/z $[\text{M} + \text{H}]^+$.

***N*-(3-((1*H*-Benzo[*d*]imidazol-1-yl)methyl)benzyl)-4-fluorobenzamide, (34).**

The title compound was synthesized following the general procedure, starting from compound **9** (60 mg, 0.25 mmol) and 4-fluorobenzoic acid (43 mg, 0.30 mmol). The crude material was purified by column chromatography using PE/EtOAc 3:7 as eluent to afford compound **34** (70 mg, 0.19 mmol, 78%) as a grey solid. Mp 116-118 °C. ¹H-NMR (300 MHz, CD₃OD): δ = 8.26 (s, 1H), 7.87-7.78 (m, 2H), 7.65 (d, *J* = 6.8 Hz, 1H), 7.41 (d, *J* = 6.8 Hz, 1H), 7.35 (d, *J* = 8.0 Hz, 2H), 7.27-7.09 (m, 6H), 5.49 (s, 2H), 4.52 (s, 2H). ¹³C-NMR (100.6 MHz, DMSO-*d*₆): δ = 165.7, 164.3 (d, *J* = 248.8 Hz), 144.7, 144.0, 140.7, 137.5, 134.1, 131.2 (d, *J* = 3.0 Hz), 130.3 (d, *J* = 9.0 Hz), 129.2, 127.1, 126.7, 126.4, 122.8, 122.0, 119.9, 115.7 (d, *J* = 21.1 Hz), 111.2, 48.1, 42.9. MS (ESI): 360 *m/z* [M + H]⁺.

***N*-(3-((1*H*-Benzo[*d*]imidazol-1-yl)methyl)benzyl)-4-cyanobenzamide, (35).**

The title compound was synthesized following the general procedure, starting from compound **9** (166 mg, 0.70 mmol) and 4-cyanobenzoic acid (123 mg, 0.84 mmol). The crude material was purified by column chromatography using PE/EtOAc 3:7 as eluent to afford compound **35** (197 mg, 0.54 mmol, 77%) as a white solid. Mp 192-194 °C. ¹H-NMR (400 MHz, CD₃OD): δ = 8.25 (s, 1H), 7.90-7.79 (m, 4H), 7.64 (d, *J* = 6.8 Hz, 1H), 7.39 (d, *J* = 6.8 Hz, 1H), 7.35-7.16 (m, 6H), 5.49 (s, 2H), 4.52 (s, 2H). ¹³C-NMR (100.6 MHz, DMSO-*d*₆): δ = 165.4, 144.7, 144.0, 140.3, 138.8, 137.5, 134.1, 132.9 (2C), 129.2, 128.6 (2C), 127.2, 126.7, 126.5, 122.8, 122.0, 119.9, 118.8, 114.1, 111.1, 48.1, 43.1. IR (KBr): $\tilde{\nu}$ 3553, 3414, 3348, 3082, 2923, 2358, 2227, 1638, 1546, 1492, 1443, 736, 742 cm⁻¹. MS (ESI): *m/z* 367 [M + H]⁺.

***N*-(3-((1*H*-Benzo[*d*]imidazol-1-yl)methyl)benzyl)-4-cyano-3-methylbenzamide, (36).**

The title compound was synthesized following the general procedure, starting from compound **9** (60 mg, 0.25 mmol) and 4-cyano-3-methylbenzoic acid (49 mg, 0.30 mmol). The crude material

1
2
3 was purified by column chromatography using PE/EtOAc 3:7 as eluent to afford compound **36** (48
4 mg, 0.13 mmol, 51%) as a yellow solid. Mp 178-180 °C. ¹H-NMR (300 MHz, DMSO-*d*₆): δ =
5 9.21 (br s, 1H), 8.40 (s, 1H), 7.90 (d, *J* = 6.9 Hz, 2H), 7.78 (d, *J* = 8.0 Hz, 1H), 7.65 (d, *J* = 5.0
6 Hz, 1H), 7.51 (d, *J* = 5.0 Hz, 1H), 7.34-7.27 (m, 2H), 7.21-7.17 (m, 4H), 5.48 (s, 2H), 4.50 (s,
7 2H). MS (ESI): 381 *m/z* [M + H]⁺.

14
15 ***N*-(3-((1*H*-Benzo[*d*]imidazol-1-yl)methyl)benzyl)-4-cyano-2-fluorobenzamide, (37).**

16
17 The title compound was synthesized following the general procedure, starting from compound **9**
18 (60 mg, 0.25 mmol) and 4-cyano-2-fluorobenzoic acid (49 mg, 0.30 mmol). The crude material
19 was purified by column chromatography using PE/EtOAc 3:7 as eluent to afford compound **37** (58
20 mg, 0.15 mmol, 60%) as a white solid. Mp 103-105 °C. ¹H-NMR (300 MHz, CD₃OD): δ = 8.28
21 (s, 1H), 7.79-7.57 (m, 4H), 7.42 (d, *J* = 5.2 Hz, 1H), 7.34 (d, *J* = 8.5 Hz, 2H), 7.27-7.19 (m, 4H),
22 5.51 (s, 2H), 4.53 (s, 2H). MS (ESI): 385 *m/z* [M + H]⁺.

30
31 ***N*-(3-((1*H*-Benzo[*d*]imidazol-1-yl)methyl)benzyl)-4-cyano-3-fluorobenzamide, (38).**

32
33 The title compound was synthesized following the general procedure, starting from compound **9**
34 (60 mg, 0.25 mmol) and 4-cyano-3-fluorobenzoic acid (50 mg, 0.30 mmol). The crude material
35 was purified by column chromatography using PE/EtOAc 3:7 as eluent to afford compound **38** (46
36 mg, 0.11 mmol, 48%) as a yellow solid. Mp 192-194 °C. ¹H-NMR (300 MHz, DMSO-*d*₆): δ =
37 9.37 (br s, 1H), 8.58 (s, 1H), 8.08 (t, *J* = 8.08 Hz, 1H), 7.95-7.80 (m, 2H), 7.65 (d, *J* = 7.6 Hz, 1H),
38 7.56 (d, *J* = 7.6 Hz, 1H), 7.43-7.16 (m, 6H), 5.53 (s, 2H), 4.45 (s, 2H). MS (ESI): 385 *m/z* [M +
39 H]⁺.

47
48
49 ***N*-(3-((1*H*-Benzo[*d*]imidazol-1-yl)methyl)benzyl)-3-morpholinopropanamide, (39).**

50
51 The title compound was synthesized following the general procedure, starting from compound **9**
52 (166 mg, 0.70 mmol) and 3-morpholinopropanoic acid (133 mg, 0.84 mmol). The crude material
53

1
2
3 was purified by column chromatography using EtOAc/MeOH 9:1 as eluent to afford compound
4
5 **39** (146 mg, 0.39 mmol, 55%) as an amorphous yellow solid. ¹H-NMR (300 MHz, CD₃OD): δ =
6
7 8.25 (s, 1H), 7.68 (t, *J* = 3.0 Hz, 1H), 7.43 (t, *J* = 3.0 Hz, 1H), 7.34-7.24 (m, 5H), 7.18 (d, *J* = 6.9
8
9 Hz, 1H), 5.48 (s, 2H), 4.34 (s, 2H), 3.58-3.50 (m, 4H), 2.60 (t, *J* = 7.0 Hz, 2H), 2.42- 2.39 (m, 4H),
10
11 2.36 (t, *J* = 7.0 Hz, 2H). IR (neat): $\tilde{\nu}$ = 3268, 2062, 1649, 1550, 1495, 1457, 1287, 1114, 743 cm⁻¹.
12
13
14 ¹. MS (ESI): *m/z* 379 [M + H]⁺.
15
16

17 **4-((*Tert*-butoxycarbonyl)amino)butanoic acid, (41).**

18
19 To a solution of 4-aminobutanoic acid **40** (200 mg, 1.94 mmol, 1 eq) in 2 M aq. NaOH (3 mL), a
20
21 solution of Boc₂O (507.50 mg, 2.33 mmol, 1.2 eq) in THF (5 mL) was added dropwise and the
22
23 reaction was stirred at rt overnight. The solvent was removed in vacuo. The aqueous layer was
24
25 acidified with 2M aq. HCl until pH 4 and extracted with EtOAc (6x). Additionally, the aqueous
26
27 layer was saturated with NaCl and extracted with THF (3x). The combined organic layers were
28
29 dried over Na₂SO₄, filtrated and concentrate in vacuo yielding the desired compound (339 mg,
30
31 1.67 mmol, 86%) as a yellow oil, which was used directly in the next step without further
32
33 purification. ¹H-NMR (300 MHz, DMSO-*d*₆): δ = 6.77 (br s, 1H), 2.92 (t, *J* = 6.3 Hz, 2H), 2.16 (t,
34
35 *J* = 6.3 Hz, 2H), 1.58 (quint, *J* = 6.9 Hz, 2H), 1.41 (s, 9H). MS (ESI): 204 *m/z* [M + H]⁺.
36
37
38
39

40 ***N*-(3-((1*H*-Benzo[*d*]imidazol-1-yl)methyl)benzyl)-4-aminobutanamide, (43).**

41
42 **Step 1:** To a solution of compound **9** (166.11 mg, 0.70 mmol, 1 eq) in dry CH₂Cl₂ (5 mL) TEA
43
44 (220 μL, 1.54 mmol, 2.2 eq), EDCI (161.28 mg, 0.84 mmol, 1.2 eq), HOBT (113.51 mg, 0.84
45
46 mmol, 1.2 eq) and compound **41** (170.71 mg, 0.84 mmol, 1.2 eq) were added in order. The resulting
47
48 mixture was stirred at room temperature for 16 h. CH₂Cl₂ was added and the organic phase was
49
50 washed with H₂O (x3), dried over Na₂SO₄ and evaporated. Purification by column chromatography
51
52 using EtOAc as eluent afforded compound **42** (168 mg, 0.40 mmol, 57%) as a yellow solid.
53
54
55
56
57
58
59
60

Step 2: To a solution of compound **42** (148 mg, 0.35 mmol, 1 eq) in CH₂Cl₂ (2.5 mL) at 0 °C CF₃COOH (1.23 mL) was added. The reaction mixture was stirred at the same temperature for 30 min and then for 3 h at rt. 2 M aq. NaOH was added until pH 7 and the aqueous layer was extracted with EtOAc (x3). The collected organic layers were dried over Na₂SO₄, filtrated and concentrated in vacuo. Purification by column chromatography using CH₃CN/NH₃ 9:1 as eluent afforded compound **43** (80 mg, 0.25 mmol, 71%) as a yellow oil. ¹H-NMR (300 MHz, CD₃OD): δ = 8.24 (s, 1H), 7.67 (d, *J* = 7.6 Hz, 1H), 7.36 (d, *J* = 7.6 Hz, 1H), 7.23-7.13 (m, 6H), 5.41 (s, 2H), 4.30 (s, 2H), 2.61 (t, *J* = 7.4 Hz, 2H), 2.19 (t, *J* = 7.4 Hz, 2H), 1.70 (quint, *J* = 6.8 Hz, 2H). IR (KBr): $\tilde{\nu}$ = 3478, 2621, 1617, 1521, 1540, 1456, 615 cm⁻¹. MS (ESI): 323 *m/z* [M + H]⁺.

***N*-(3-((1*H*-Benzo[*d*]imidazol-1-yl)methyl)benzyl)formamide, (44).**

To a solution of amine **9** (500 mg, 2.11 mmol, 1 eq) in formic acid (1.86 mL) acetic anhydride (1.58 mL, 16.86 mmol, 8 eq) was added dropwise at 0 °C. After ten min, the mixture was allowed to reach room temperature and was stirred for 3 h. Then, water was added and the mixture was stirred for additional 10 min. The volatile was removed, affording compound **44** (548 mg, 2.07 mmol, 98%) as a yellow oil. ¹H-NMR (300 MHz, CD₃OD): δ = 8.20 (s, 1H), 8.12 (s, 1H), 7.66 (d, *J* = 7.5 Hz, 1H), 7.31 (d, *J* = 7.8 Hz, 1H), 7.18-7.14 (m, 5H), 7.03 (s, 1H), 5.27 (s, 2H), 4.28 (s, 2H). IR (neat): $\tilde{\nu}$ = 3256, 3051, 2861, 1664, 1494, 1457, 1381, 1261, 1007, 738, 698 cm⁻¹. MS (ESI): 266 *m/z* [M + H]⁺.

1-(3-(Isocyanomethyl)benzyl)-1*H*-benzo[*d*]imidazole, (45).

Compound **44** (500 mg, 1.89 mmol, 1 eq) was dissolved in dry CH₂Cl₂ (7 mL) and TEA (1.3 mL, 9.43 mmol, 5 eq) was added at 0 °C and under nitrogen. A solution of POCl₃ (259 μL, 2.83 mmol, 1.5 eq) in dry CH₂Cl₂ (4 mL) was added dropwise and the reaction was stirred for 1.5 h at 0 °C. Aqueous saturated NaHCO₃ solution was then added and the mixture was left to reach room

1
2
3 temperature and stirred for additional 10 min. Then, the reaction was extracted with CH₂Cl₂, dried
4 over Na₂SO₄ and evaporated, yielding compound **45** (205.4 mg, 0.83 mmol, 44%) as an amorphous
5 yellow solid. ¹H-NMR (300 MHz, CD₃OD): δ = 7.88 (s, 1H), 7.45 (dd, *J*_s = 6.8, 2.5 Hz, 1H), 7.29-
6 7.17 (m, 5H), 7.04 (m, 2H), 5.23 (s, 2H), 4.45 (s, 2H). IR (KBr): $\tilde{\nu}$ = 2927, 2854, 2671, 2159, 1617,
7 1494, 1437, 1266, 746 cm⁻¹.
8
9

10
11
12
13
14 ***N*-(3-((1*H*-Benzo[*d*]imidazol-1-yl)methyl)benzyl)-2-acetamidoacetamide, (46).**

15
16 To a solution of compound **45** (197.6 mg, 0.8 mmol, 1 eq) in MeOH (1.4 mL) and water (0.5 mL)
17 acetic acid (45 μL, 0.8 mmol, 1 eq), NH₄Cl (128.3 mg, 2.4 mmol, 3 eq), TEA (111 μL, 0.8 mmol,
18 1 eq) and paraformaldehyde (38.4 mg, 0.80 mmol, 1 eq) were added in order. The mixture was
19 heated at 65 °C for 8 h. Then, water was added and the aqueous phase was extracted with EtOAc
20 (3x). The organic phases were collected, dried over Na₂SO₄ and evaporated. The crude product
21 was purified by column chromatography using EtOAc/MeOH 9:1 as eluent, affording compound
22 **46** (80 mg, 0.25 mmol, 30%) as a white solid. Mp 164-166 °C. ¹H-NMR (300 MHz, CD₃OD): δ =
23 8.30 (s, 1H), 7.66 (d, *J* = 6.7 Hz, 1H), 7.41 (d, *J* = 6.2 Hz, 1H), 7.24-7.18 (m, 5H), 7.15 (s, 1H),
24 5.44 (s, 2H), 4.35 (s, 2H), 3.85 (s, 2H), 1.99 (s, 3H). IR (KBr): $\tilde{\nu}$ = 3476, 3415, 3228, 3054, 2927,
25 2811, 1617, 1548, 1286 cm⁻¹. MS (ESI): 337 *m/z* [M + H]⁺.
26
27
28
29
30
31
32
33
34
35
36
37
38
39

40 ***N*-(2-((3-((1*H*-Benzo[*d*]imidazol-1-yl)methyl)benzyl)amino)-2-oxoethyl)benzamide, (47).**

41
42 The title compound was synthesized following the procedure described for compound **46**. The
43 crude material was purified by column chromatography using EtOAc/MeOH 9:1 as eluent to afford
44 compound **47** (101.9 mg, 0.26 mmol, 32%) as a white solid. Mp 136-138 °C. ¹H-NMR (300 MHz,
45 CD₃OD): δ = 8.28 (s, 1H), 7.89 (d, *J* = 7.9 Hz, 2H), 7.66 (d, *J* = 7.7 Hz, 1H), 7.52-7.42 (m, 3H),
46 7.26-7.18 (m, 6H), 7.12 (s, 1H), 5.46 (s, 2H), 4.37 (s, 2H), 4.07 (s, 2H). IR (KBr): $\tilde{\nu}$ = 3465, 3415,
47 3081, 2931, 1686, 1453, 1437, 1207, 1142, 737, 725 cm⁻¹. MS (ESI): 399 *m/z* [M + H]⁺.
48
49
50
51
52
53
54
55
56
57
58
59
60

3-(((5-Bromo-2-nitrophenyl)amino)methyl)benzonitrile, (50).

To a solution of 2,4-dibromo-1-nitrobenzene **48** (100 mg, 0.36 mmol, 1 eq) in DMSO (1 mL), K₂CO₃ (73 mg, 0.53 mmol, 1.5 eq) and 3-(aminomethyl)benzonitrile **49** (51 mg, 0.39 mmol, 1.01 eq) were added in order. The reaction mixture was stirred at 72 °C overnight. EtOAc was added and the organic layer was washed with aqueous saturated NaHCO₃ (3x), dried over Na₂SO₄, filtered and concentrated in vacuo. Purification by silica gel column chromatography using PE/EtOAc 95:5 as eluent afforded compound **50** (15 mg, 0.05 mmol, 13%) as a yellow solid. Mp 196-198 °C. ¹H-NMR (300 MHz, CDCl₃): δ = 8.42 (s, 1H), 8.08 (d, *J* = 7.8 Hz, 1H), 7.62-7.49 (m, 2H), 7.51 (d, *J* = 7.8 Hz, 1H), 6.88-6.83 (m, 2H), 4.57 (d, *J* = 4.7 Hz, 2H). IR (KBr): $\tilde{\nu}$ = 3390, 2921, 2229, 1962, 1890, 1520, 1408, 1257, 1049, 750, 618 cm⁻¹. MS (ESI): 332 *m/z* [M + H]⁺.

3-(((6-Bromo-1H-benzo[d]imidazol-1-yl)methyl)benzonitrile, (51).

To a solution of compound **50** (0.93 g, 56.24 mmol, 1 eq) in formic acid (29 mL), Fe (3.14 g, 56.24 mmol, 20 eq) was added. The reaction mixture was heated to 85 °C for 16 h. MeOH (29 mL) was added, the reaction was filtered and the filtrate concentrate in vacuo. The crude material was purified by silica gel column chromatography using PE/EtOAc 4:6 as eluent yielding a yellow solid (1.21 g, 38.81 mmol, 69%). Mp 123-125 °C. ¹H-NMR (300 MHz, CDCl₃): δ = 8.00 (s, 1H), 7.62 (m, 2H), 7.42-7.26 (m, 5H), 5.35 (s, 2H). IR (KBr): $\tilde{\nu}$ = 3063, 2921, 2722, 2356, 2228, 1699, 1493, 1462, 1361, 1283, 767, 690 cm⁻¹. MS (ESI): 313 *m/z* [M + H]⁺.

(3-(((6-Bromo-1H-benzo[d]imidazol-1-yl)methyl)phenyl)methanamine, (52).

Compound **52** was synthesized as previously reported for the preparation of compound **9**, starting from compound **51** (350 mg, 1.17 mmol). The crude material was purified by column chromatography using EtOAc/MeOH 7:3 to obtain the desired compound (147 mg, 0.47 mmol, 40%) as a yellow oil. ¹H-NMR (300 MHz, CD₃OD): δ = 8.21 (s, 1H), 7.55 (t, *J* = 7.1 Hz, 1H),

7.36 (dd, $J_s = 1.4, 7.4$ Hz, 1H), 7.23-7.17 (m, 4H), 7.05 (s, 1H), 5.32 (s, 2H), 3.7 (s, 2H). IR (KBr): $\tilde{\nu} = 3521, 3444, 2922, 2855, 1496, 1562, 1458, 1367, 745$ cm⁻¹. MS (ESI): 316 m/z [M + H]⁺.

4-Bromo-*N*-(3-((6-bromo-1*H*-benzo[*d*]imidazol-1-yl)methyl)benzyl)-1*H*-pyrrole-2-carboxamide, (53).

The title compound was synthesized following the general procedure, starting from compound **52** (100 mg, 0.32 mmol) and 4-bromo-1*H*-pyrrole-2-carboxylic acid (71 mg, 0.38 mmol). The crude material was purified by column chromatography using PE/EtOAc 3:7 as eluent to afford compound **53** (61 mg, 0.12 mmol, 39%) as a white solid. Mp 200-202 °C. ¹H-NMR (300 MHz, CD₃OD): $\delta = 8.26$ (s, 1H), 7.65 (d, $J = 7.7$ Hz, 1H), 7.55 (d, $J = 7.7$ Hz, 1H) 7.31-7.13 (m, 5H), 6.91 (s, 1H), 6.73 (s, 1H), 7.15 (s, 2H), 4.45 (s, 2H). ¹³C-NMR (100.6 MHz, DMSO-*d*₆): $\delta = 161.2, 144.8, 144.0, 140.3, 138.0, 134.7, 129.7, 127.0, 126.9, 126.8, 125.2, 122.8, 122.2, 121.8, 118.7, 117.9, 111.2, 94.8, 50.4, 42.9$. IR (KBr): $\tilde{\nu} = 3484, 3407, 3224, 3119, 3291, 2769, 1564, 1525, 1459, 749$ cm⁻¹. MS (ESI): 489 m/z [M + H]⁺.

In vitro metabolism studies

***In vitro* metabolism in mouse liver microsomes**

Mouse liver microsomes (MLM), (pooled male mouse CD-1, protein concentration: 20 mg/mL) were purchased from Corning B.V. Life Sciences (Amsterdam, The Netherlands) and used throughout this study. The standard incubation mixture (250 μ L final volume), was carried out in a 50 mM TRIS (tris[hydroxymethyl]aminomethane) buffer (pH 7.4) containing 3.3 mM MgCl₂, 1.3 mM β -NADP-Na₂, 3.3 mM glucose 6-phosphate, 0.4 Units/mL glucose 6-phosphate dehydrogenase (NADPH regenerating system), 5 μ L of acetonitrile (1% of total volume), and the substrate compounds at a concentration of 50 μ M. After pre-equilibration of the mixture, an appropriate volume of MLM suspension was added to give a final protein concentration of 1

1
2
3 mg/mL. The mixture was shaken for 60 min at 37 °C. Control incubations were carried out without
4
5 the presence of MLM suspension or cofactors. When metabolic activation was studied, 3 mM GSH
6
7 trapping agent was added in the incubation mixture. Each incubation was stopped by addition of
8
9 250 μ L ice-cold acetonitrile, vortexed and centrifuged at 13000 r.p.m. for 10 min.
10
11

12 **CYP inhibition: aminopyrine *N*-demethylase assay**

14 Aminopyrine *N*-demethylase activity was determined by detecting the amount of formaldehyde
15 produced by rat liver microsomes (RLM). The incubation was carried out in Tris-HCl buffer (50
16 mM, pH 7.4) supplemented with 150 mM KCl and 10 mM MgCl₂. The incubation contained 1
17 mM aminopyrine, acetonitrile (1% final volume), and 1 mg/mL of RLM in a total volume of 180
18
19 μ L. Increasing concentrations of **10**, **23** and **35** (0.01, 1, 5, 10, 25, 50, 75, and 100 μ M) were added
20
21 to the incubation mixture to inhibit aminopyrine *N*-demethylase activity. After 3 min pre-
22
23 incubation at 37 °C, the reaction was initiated by adding the β -NADPH (3 mM) and carried out at
24
25 37 °C for 15 min with moderate shaking. The reaction was then quenched by addition of 90 μ L of
26
27 20% (w/v) cold TCA solution. After centrifugation at 13000 r.p.m. for 10 min, a 240 μ L aliquot of
28
29 the protein-free supernatant was treated with 120 μ L of Nash reagent and incubated at 37 °C for
30
31 40 min. The absorbance intensity of the resultant solution was determined at 412 nm, subtracting
32
33 the blank sample absorbance (without β -NADPH). The concentration of formaldehyde was
34
35 quantified (nmol/min/mg) by comparison with a standard curve prepared from commercially
36
37 available formaldehyde solution freshly standardized by iodometric titration. IC₅₀ values were
38
39 calculated by using GraphPad Prism software (GraphPad Software, Inc., USA). Nash reagent: 3.75
40
41 g ammonium acetate, 50 μ l glacial acetic acid, and 75 μ L acetylacetone were dissolved in 25 mL
42
43 of deionized water. The solution was freshly prepared and used only for one day.
44
45
46
47
48
49
50
51
52

53 **Biology**

Ligand binding experiments

Recombinant human IDO1 (rhIDO1) was purchased from Proteros Biostructures GmbH, (Martinsried, Germany). Experiments to assess K_d values were conducted using Monolith NT.115 instrument (NanoTemper Technologies, Munich, Germany). Fluorescence labeling of rhIDO1 was performed following the protocol for *N*-hydroxysuccinimide (NHS) coupling of RED dye NT650 (NanoTemper Technologies, Munich, Germany) to lysine residues. Briefly, 100 μ L of a 20 μ M solution of rhIDO1 protein in MES buffer (25 mM MES, 150 mM KCl, pH 6.5) was mixed with 100 μ L of 80 μ M NT650-NHS fluorophore (NanoTemper Technologies, Munich, Germany) and incubated for 30 min at room temperature in the dark. Unbound fluorophores were removed by size-exclusion chromatography with MST buffer (50 mM TRIS, 150 mM NaCl, 10 mM $MgCl_2$, pH 7.4, 0.05% Tween20) as running buffer. The real concentration of each element of the sample, such as protein, heme group and RED dye, and the *degree of labeling (DoL)* were determined using extinction coefficient $\epsilon_{280} = 51,380 \text{ M}^{-1} \text{ cm}^{-1}$ for rhIDO1, $\epsilon_{405} = 159,000 \text{ M}^{-1} \text{ cm}^{-1}$ for rhIDO1 heme group and $\epsilon_{650} = 195,000 \text{ M}^{-1} \text{ cm}^{-1}$ for NT650 fluorophore, with a correction factor (F_{corr}) of 0.04 at 280 nm, using $C_{prot} = [A_{280} - (A_{650} \times F_{corr}) / \epsilon_{280} \times l]$, and *DoL* resulted between 0.6 and 0.8. Compound pre-dilutions were prepared for MST experiments by 16-fold 1:1 serial dilutions in assay buffer containing 4% DMSO in PCR tubes supplied by NanoTemper Technologies to yield final volumes of 10 μ L. NT650-rhIDO1 solution 10 μ L was added to each compound dilution and mixed to reach a final NT650-rhIDO1 concentration of 50 nM, including 2% DMSO, 2 mM DTT and a reaction volume of 20 μ L. After 10 min incubation, these samples were loaded into 16 premium-coated capillaries and inserted in the chip tray of the MST instrument for thermophoresis analysis and K_d evaluation. MST signals were recorded at Medium MST power (compounds **1** and **10**) and 20% LED power. Each compound was tested in three independent

1
2
3 experiments and recorded data were processed with NanoTemper *MO.Affinity Analysis* software
4
5 v2.3 in *Manual* mode setting the hot region between 19-20 seconds. Confidence values (\pm) are
6
7 indicated next to K_d value, showing the range where the K_d falls with a 68% of certainty.
8
9

10 **Cell culture**

11
12 Human A375 cells were cultured in DMEM medium with high glucose (4.5 g/L), containing 10%
13
14 heat inactivated fetal bovine serum (FBS), 2 mM L-glutamine 100 U/mL of penicillin and 10
15
16 $\mu\text{g/mL}$ of streptomycin (GE Healthcare, Milan, Italy). Human HeLa, HepG2 and MCF-7 cells
17
18 were cultured in EMEM medium containing 10% FBS, 2 mM L-glutamine 100 U/mL of penicillin
19
20 and 10 $\mu\text{g/mL}$ of streptomycin (GE Healthcare, Milan, Italy). Human LXF-289 and DAN-G cells
21
22 were cultured in RPMI medium containing 10% FBS, 2 mM L-glutamine 100 U/mL of penicillin
23
24 and 10 $\mu\text{g/mL}$ of streptomycin (GE Healthcare, Milan, Italy).
25
26

27
28 Cells of P1.HTR, a highly transfectable clonal variant of mouse mastocytoma P815,⁵⁰ were
29
30 transfected by electroporation with plasmid constructs coding for mouse IDO1 (P1.IDO1) or TDO
31
32 (P1.TDO). Stable transfectant cell lines were obtained by puromycin selection. Both cell lines were
33
34 cultured in Iscove's Modified Dulbecco's Medium (Gibco, Invitrogen CA, USA) supplemented
35
36 with 10% FCS (Gibco, Invitrogen CA, USA), 1 mM glutamine (Gibco, Invitrogen CA, USA) and
37
38 penicillin/streptomycin (Gibco, Invitrogen CA, USA).
39
40
41

42
43 Peripheral blood samples were collected from a cohort of 16 patients with different stages of
44
45 pancreatic ductal adenocarcinoma admitted at the Unit of General and Pancreatic Surgery of the
46
47 Azienda Ospedaliera Universitaria Integrata of Verona before surgical resection or from healthy
48
49 donors. No subject was undergoing therapy at the time of sample collection. PBMCs were isolated
50
51 by Ficoll-Hypaque (GE Healthcare). Monocytes were isolated from PBMCs by using CD14
52
53 MicroBeads (Miltenyi Biotech) according to manufacturer's instructions with at least 95% cell
54
55
56
57
58
59
60

1
2
3 purity, as evaluated by flow cytometry. Cells were cultured in a humidified atmosphere (5% CO₂,
4
5 37 °C).
6

7 **Cell cytotoxicity**

8
9
10 Cell viability was measured by the 3-(4,5-dimethylthiazol-2-yl)-2,5-diphenyl-tetrazolium bromide
11 (MTT) assay, as previously described.⁵¹ A375 cells were seeded (0.5 x 10⁵ cells/well) in 24-well
12
13
14 plates and treated with each compound (1 μM) for 48 h at 37 °C in a 5% CO₂ humidified incubator.
15
16
17 The percentage of cell viability was calculated as $[100 (x-y)/(z-y)]$, where x, y, and z were the
18
19 absorbance read in compound-treated, resting and compound-untreated cells, respectively.
20
21

22 **Monocytes viability assay**

23
24 Purified monocytes from HD were treated or not with increasing concentration of epacadostat,
25
26 compounds **10** and **23**. Purified monocytes from PDAC patients were treated or not with 30 μM
27
28 epacadostat, compounds **10** and **23**. Following 24 h, cells were stained with Annexin V using the
29
30 Annexin V Apoptosis Detection Kit APC (eBioscience, Thermo Fisher Scientific) and 7-AAD (BD
31
32 Biosciences). Cell viability was evaluated on AnnexinV^{neg}7AAD^{neg} monocytes by flow cytometry
33
34 and FlowJo software (TreeStar).
35
36
37

38 **Cellular IDO1 enzymatic assay**

39
40 The enzymatic activity of IDO1 was evaluated by measuring the levels of L-Kyn into A375 cell
41
42 media, as previously described.⁵² A375 cells (3x10⁴) were seeded in a 24-well culture plate (500
43
44 μL/well) and grown overnight. DMSO dilutions (1 μM) of each compound in a total volume of
45
46 500 μL culture medium including human IFN-γ (1000 U/mL final concentration) per well were
47
48 added into wells containing the cells. All compounds were dissolved in DMSO (Sigma–Aldrich).
49
50
51 The DMSO final concentration in cell culture medium was always 0.1%. Equivalent amount of
52
53
54 DMSO was always added to drug untreated controls. After 48 h incubation, cell medium was
55
56
57
58
59
60

1
2
3 collected, deproteinized by 20% (v/v) aqueous CCl_3COOH , centrifuged at 13,200 rpm for 10 min,
4 and the amounts of L-Kyn in A375 cell media were quantified with HPLC. 20 μL of supernatants
5 were injected by a multi-sampler (Beckman Coulter, Milan, Italy) into a HPLC-UV system
6 (System Gold, Beckman Coulter), equipped with a C-18 sphereClone ODS analytical column (5
7 μm particle size, 250 mm x 4.0 mm; Phenomenex, Torrance, CA, USA). The mobile phase (50
8 mM potassium dihydrogen phosphate, 10% v/v acetonitrile; pH 4.8) was delivered at a flow-rate
9 of 1 mL/min at room temperature, and the absorbance was measured at 330 nm. Amounts of L-
10 Kyn in A375 cell media were quantified on the basis of a calibration curve obtained using the same
11 HPLC-UV experimental setting. To calculate IC_{50} values, IFN- γ -stimulated A375 cells were
12 incubated with increasing concentrations (0.001-3 μM) of compounds for 48 h and L-Kyn levels
13 were evaluated by HPLC, as reported above. The determination of inhibitors activity on HeLa,
14 HepG2, LXF-289, MCF-7 and DAN-G cell lines was performed similarly to A375 cells.

30 **IDO1 and TDO selectivity assay**

31
32 In every cellular assay, P1 transfected cells were used at a passage number not exceeding the 10th.
33 Dose-response curves for extrapolating the cellular IC_{50} were built by incubating 1×10^5 P1.IDO1
34 or P1.TDO cells in a final volume of 400 μL with 3-fold serial dilutions of each compound for 16
35 h in a 48-well plate. The control was represented by cells incubated with an equivalent volume of
36 DMSO, the vehicle in which compounds have been solubilized. After the incubation, supernatants
37 of cell cultures were recovered and L-Kyn concentration was detected by HPLC-UV. Every cell
38 assay was conducted in triplicate and repeated three times. Detection of L-Kyn concentrations was
39 performed by using a Perkin Elmer, series 200 HPLC instrument (MA, USA). A Kinetex® C18
40 column (250×4.6 mm, 5 μm , 100 Å; Phenomenex, USA), maintained at the temperature of 25 °C
41 and pressure of 1800 PSI, was used. A sample volume of 300 μL was injected and eluted by a
42
43
44
45
46
47
48
49
50
51
52
53
54
55
56
57
58
59
60

1
2
3 mobile phase containing 10 mM NaH₂PO₄ pH 3.0 (99%) and methanol (1%) (Sigma-Aldrich, MO,
4 USA), with a flow rate of 1 mL/min. L-Kyn was detected at 360 nm by an UV detector. The
5 software TURBOCHROM 4 was used for evaluating the concentration of L-Kyn in samples by
6 mean of a calibration curve. The detection limit of the analysis was 0.05 μM.
7
8
9
10

11 **T cell proliferation assay**

12
13
14 PBMCs were isolated from leukocytes-enriched buffy coats from HD (Transfusion Centre,
15 University and Hospital Trust of Verona, Italy), stained with 1 μM of CellTrace Violet (Thermo
16 Fisher Scientific) in PBS and followed by 5 min incubation at 37 °C, protected from light. Labelled
17 PBMCs were stimulated with coated 0.6 μg/mL anti-CD3 (clone OKT-3, eBioscience, Thermo
18 Fisher Scientific) and 5 μg/mL anti-CD28 (clone CD28.2, eBioscience, Thermo Fisher Scientific)
19 for 4 days and co-cultured with monocytes pre-treated or not with 30 μM of epacadostat **1**,
20 compounds **10** and **23** for 24 h at 3:1 ratio (monocyte:PBMCs). Cell cultures were incubated at
21 37 °C and 8% CO₂ in L-arginine and L-glutamine-free-RPMI (Biochrom), supplemented with 2
22 mM L-glutamine (Euroclone), 150 μM L-arginine (Sigma-Aldrich), 10% FBS (Superior, Merck),
23 10 U/mL penicillin and streptomycin (Euroclone), and 0.1 mM HEPES (Euroclone). At the end of
24 the co-culture, cells were stained with PE-Cy7 conjugated anti-CD3 (UCHT1, eBioscience,
25 Thermo Fisher Scientific), and CellTrace signal of CD3⁺ gated lymphocytes were analysed by
26 flow cytometry and FlowJo software (Tree Star).
27
28
29
30
31
32
33
34
35
36
37
38
39
40
41
42
43
44

45 **Western Blot**

46
47 5x10⁶ monocytes isolated from HD and PDAC samples were lysed in RIPA buffer with the
48 addition of protease inhibitor cocktail tablets (Roche) and sodium vanadate. SDS-PAGE was
49 performed loading 40 μg of protein lysates on 10% denaturing SDS polyacrylamide gel and
50 transferred on PVDF membrane (Millipore). Membrane was blocked in Tris-buffered saline plus
51
52
53
54
55
56
57
58
59
60

0.01% Tween-20 and 5% non-fat milk and incubated with rabbit anti-human IDO (D5J4E, Cell Signaling Technologies), followed by the secondary incubation with goat anti-rabbit IgG antibody, horseradish peroxidase (HRP)-conjugated (Millipore).

Animal studies

Animal care was in compliance with Italian regulations on protection of animals used for experimental purposes and were authorized by the Ministry of Health (259/2019 DB064.44 of 28/03/2019).

Pharmacokinetic-Pharmacodynamic studies

8 Weeks-old male BALB/C mice (n=8; Envigo) were maintained under 12-h light/dark cycle at 21 ± 1 °C and $50 \pm 5\%$ humidity. Mice were starved 8 h before the single dose administration of epacadostat (INCB24360) and **23**.⁴⁰ INCB24360, used as a positive control, was administered 50 mg/kg and **23** intravenously at the dose of 10 mg/kg. The blood was collected from the eye by a retro-orbital puncture at different time points (2, 5, 15, 30 min, 1 h, 3 h, 8 h, 24 h), centrifuged at 8679 rpm for 15', separating the clot from the plasma, and then used for LC/MS analysis.

Pharmacokinetic analysis

After 10 mg/Kg endovenous administration of **10** and **23** blood was drawn after 2, 5, 15, 30, 60, 180 min and 24 h. Aliquots of plasma samples (50 μ L) were diluted by adding 100 μ L of acetonitrile. Samples were homogenized and centrifuged at 13000 r.p.m. for ten min and supernatants (5 μ L) were injected into LC-HRMS system. Plasma calibration standards were prepared by spiking appropriate amounts of analytes into blank plasma. The calibration curves ($y = ax + b$), were constructed from the peak area versus plasma concentration using the weighted ($1/x$) linear least-squares regression method (calibration range 0.1-5000 μ g/L).

L-Kyn levels analysis

1
2
3 After 10 mg/kg endovenous administration of **10**, **23**, epacadostat (control) blood was drawn after
4
5 2, 5, 15, 30, 60, 180 min and 24 h. Aliquots of plasma samples (50 μ L) were diluted by adding 100
6
7 μ L of acetonitrile. Samples were homogenized and centrifuged at 13000 r.p.m. for 10 min and
8
9 supernatants (5 μ L) were injected into LC-HRMS system. The % of L-Kyn was calculated
10
11 considering 100% the area of the analyte before the administration.
12
13
14
15
16

17 ASSOCIATED CONTENT

18 **Supporting Information.**

19 The Supporting Information is available free of charge.
20
21

22
23 Molecular modelling, NMR spectra of compounds **10**, **23** and **35**, dose-response curves of the
24
25 selected compounds in A375, P1.IDO1 and P1.TDO cell lines, metabolic stability data, structural
26
27 characterization of metabolites by HRMS and *in vivo* PK/PD evaluation of compound **23**.
28
29

30
31 Molecular formula strings.
32
33

34 AUTHOR INFORMATION

35 **Corresponding Authors**

36
37 Dr. Alberto Massarotti
38
39

40
41 Dept. of Pharmaceutical Sciences
42
43

44
45 Università del Piemonte Orientale
46
47

48
49 Largo Donegani, 2 – 28100 Novara
50
51

52
53 Phone: 0039-0321-375753
54
55

56
57 Fax: 0039-0321-375821
58
59

60
61 e-mail: alberto.massarotti@uniupo.it
62

1
2
3 Prof. Tracey Pirali

4
5 Dept. of Pharmaceutical Sciences

6
7 Università del Piemonte Orientale

8
9 Largo Donegani, 2 – 28100 Novara

10
11 Phone: 0039-0321-375852

12
13 Fax: 0039-0321-375821

14
15 e-mail: tracey.pirali@uniupo.it

16
17
18
19
20
21
22 **Author Contributions**

23
24 The manuscript was written through contributions of all authors. All authors have given approval
25 to the final version of the manuscript. ‡These authors contributed equally. *These authors
26 contributed equally.
27
28
29
30

31
32 **Notes**

33
34 The authors declare no competing financial interest.
35
36
37
38
39
40

41 **ACKNOWLEDGMENT**

42
43 We gratefully acknowledge Salvatore Terrazzino for support in the PK data analysis. M. S. is
44 supported by Fondazione AIRC (Associazione Italiana per la Ricerca sul Cancro) fellowship for
45 Italy (Rif. 22568). T.P., S.A., S.F., M.T.P. and S.U. gratefully acknowledge Ministero
46 dell'Istruzione, dell'Università e della Ricerca (MIUR) for financial support (PRIN 2017 N°
47 2017WJZ9W9). This work was partially supported by S.U. grant (21509) from Fondazione AIRC.
48
49
50
51
52
53
54
55
56
57
58
59
60

1
2
3 ABBREVIATIONS
4

5 AO, aldehyde oxidase; Boc₂O, di-*tert*-butyl dicarbonate; CD3, cluster of differentiation 3; CD28,
6 cluster of differentiation 28; CDCl₃, deuterated chloroform; CD₃OD, deuterated methanol;
7 CH₂Cl₂, dichloromethane; CTLA-4, cytotoxic T-lymphocyte antigen 4; CYP, cytochrome P450;
8 DC, dendritic cells; DKIE, deuterium kinetic isotope effect; DMEM, Dulbecco's modified eagle
9 medium; DMSO-*d*₆, deuterated dimethyl sulfoxide; DoL, degree of labeling; EDCI, 1-ethyl-3-(3-
10 dimethylaminopropyl)carbodiimide; EtOAc, ethyl acetate; FBS, fetal bovine serum; GCN2,
11 general control nonderepressible 2; GSH, glutathione; HOBt, hydroxybenzotriazole; HD, healthy
12 donor; HPLC, high performance liquid chromatography; HRP, horseradish peroxidase; IC₅₀, half
13 maximum inhibitory concentration; IDO1, indoleamine 2,3-dioxygenase-1; IDO2, indoleamine
14 2,3-dioxygenase-2; IFN γ , interferon gamma; IR, infrared; L-Kyn, L-kynurenine; LC-HRMS,
15 liquid chromatography - high resolution mass spectrometry; HPLC-UV, high pressure liquid
16 chromatography - ultraviolet; MCR, multicomponent reaction; MD, Molecular dynamics;
17 MDSCs, monocytic myeloid-derived suppressor cells; MeOH, methanol; MLM, mouse liver
18 microsomes; Mp, melting point; mTOR1, mammalian target of rapamycin complex 1; MST,
19 MicroScale Thermophoresis; MTT, 3-(4,5-dimethylthiazol-2-yl)-2,5-diphenyl-tetrazolium
20 bromide; NADPH, nicotinamide adenine dinucleotide phosphate; NHS, *N*-hydroxysuccinimide;
21 PBMCs, peripheral blood mononuclear cells; PBS, phosphate-buffered saline, PDAC, pancreatic
22 ductal adenocarcinoma; PD, pharmacodynamics; PD-1, programmed cell death protein 1; PE,
23 petroleum ether; PK, pharmacokinetic; rhIDO1, recombinant human IDO1; RIPA,
24 radioimmunoprecipitation assay; RMSD, root mean square deviation; RLM, rat liver microsomes;
25 RT-PCR, reverse transcriptase-polymerase chain reaction; SAR, structure activity relationship;
26 SEM, standard error of the mean; SDS, sodium dodecyl sulphate; TEA, triethylamine; THF,
27
28
29
30
31
32
33
34
35
36
37
38
39
40
41
42
43
44
45
46
47
48
49
50
51
52
53
54
55
56
57
58
59
60

1
2
3 tetrahydrofuran; TLC, thin layer chromatography; Treg, regulatory T cells; L-Trp, L-tryptophan;
4
5 TDO, tryptophan 2,3-dioxygenase.
6
7
8
9

10
11 REFERENCES

- 12
13 1. a) Ribas, A.; Wolchok, J. D. Cancer immunotherapy using checkpoint blockade. *Science*
14 **2018**, *359*, 1350-1355;
15
16 b) Wilkinson, R. W.; Leishman, A. J. Further advances in cancer immunotherapy: going
17 beyond checkpoint blockade. *Front. Immunol.* **2018**, *9*, 1082-1085.
18
19 2. a) Hodi, F. S.; O'Day, S. J.; McDermott, D. F.; Weber, R. W.; Sosman, J. A.; Haanen, J.
20 B.; Gonzalez, R.; Robert, C.; Schadendorf, D.; Hassel, J. C.; Akerley, W.; van den
21 Eertwegh, A. J. M.; Lutzky, J.; Lorigan, P.; Vaubel, J. M.; Linette, G. P.; Hogg, D.;
22 Ottensmeier, C. H.; Lebbe, C.; Peschel, C.; Quirt, I.; Clark, J. I.; Wolchok, J. D.; Weber, J.
23 S.; Tian, J.; Yellin, M. J.; Nichol, G. M.; Hoos, A.; Urban, W. J. Improved survival with
24 ipilimumab in patients with metastatic melanoma. *N. Engl. J. Med.* **2010**, *363*, 711-723;
25
26 b) Robert, C.; Schachter, J.; Long, G. V.; Arance, A.; Grob, J. J.; Mortier, L.; Daud, A.;
27 Carlino, M. S.; McNeil, C.; Lotem, M.; Larkin, J.; Lorigan, P.; Neyns, B.; Blank, C. U.;
28 Hamid, O.; Mateus, C.; Shapira-Frommer, R.; Kosh, M.; Zhou, H.; Ibrahim, N.;
29 Ebbinghaus, S.; Ribas, A. Pembrolizumab versus ipilimumab in advanced melanoma. *N.*
30 *Engl. J. Med.* **2015**, *372*, 2521-2532;
31
32 c) Kazandjian, D.; Suzman, D. L.; Blumenthal, G.; Mushti, S.; He, K.; Libeg, M.; Keegan,
33 P.; Pazdur, R. FDA approval summary: nivolumab for the treatment of metastatic non-
34 small cell lung cancer with progression on or after platinum-based chemotherapy.
35 *Oncologist* **2016**, *21*, 634-642.
36
37
38
39
40
41
42
43
44
45
46
47
48
49
50
51
52
53
54
55

- 1
2
3 d) Pacheco, J. M.; Camidge, D. R.; Doebele, R. C.; Schenk, E. A changing of the guard:
4 immune checkpoint inhibitors with and without chemotherapy as first line treatment for
5 metastatic non-small cell lung cancer. *Front. Oncol.* **2019**, *9*, 195-207.
6
7
8
9
10 3. a) Jenkins, R. W.; Barbie, D. A.; Flaherty, K. T. Mechanisms of resistance to immune
11 checkpoint inhibitors. *Br. J. Cancer* **2018**, *118*, 9-16;
12
13 b) Sharma, P.; Hu-Lieskovan, S.; Wargo, J. A.; Ribas, A. Primary, adaptive, and acquired
14 resistance to cancer immunotherapy. *Cell* **2017**, *168*, 707-723.
15
16 c) Restifo, N. P.; Smyth, M. J.; Snyder A. Acquired resistance to immunotherapy and future
17 challenges. *Nat. Rev. Cancer* **2016**, *16*, 121-126.
18
19
20
21
22
23 4. a) Weinmann, H. Cancer immunotherapy: selected targets and small-molecule modulators.
24 *ChemMedChem* **2016**, *11*, 450-466;
25
26 b) Melero, I.; Berman, D. M.; Aznar, M. A.; Korman, A. J.; Pérez Gracia, J. L.; Haanen, J.
27 Evolving synergistic combinations of targeted immunotherapies to combat cancer. *Nat.*
28 *Rev. Cancer* **2015**, *15*, 457-472;
29
30 c) Antonia, S. J.; Larkin, J.; Ascierto, P. A. Immuno-oncology combinations: a review of
31 clinical experience and future prospects. *Clin. Cancer Res.* **2014**, *20*, 6258-6268.
32
33
34
35 5. a) Prendergast, G. C.; Mondal, A.; Dey, S.; Laury-Kleintop, L. D.; Muller, A. J.
36 Inflammatory reprogramming with IDO1 inhibitors: turning immunologically
37 unresponsive 'cold' tumors 'hot'. *Trends Cancer* **2018**, *4*, 38-58.
38
39 b) Munn, D. H.; Mellor, A. L. IDO and tolerance to tumors. *Trends Mol. Med.* **2004**, *10*,
40 15-18;
41
42
43
44
45
46
47
48
49
50
51
52
53
54
55
56
57
58
59
60

- 1
2
3 c) Uyttenhove, C.; Pilotte, L.; Theate, I.; Stroobant, V.; Colau, D.; Parmentier, N.; Boon,
4 T.; Van den Eynde, B. J. Evidence for a tumoral immune resistance mechanism based on
5 tryptophan degradation by indoleamine 2,3-dioxygenase. *Nat. Med.* **2003**, *9*, 1269-1274.
6
7
8
9
10 6. Metz, R.; Rust, S.; Duhadaway, J. B.; Mautino, M. R.; Munn, D. H.; Vahanian, N. N.; Link,
11 C. J.; Prendergast, G. C. IDO inhibits a tryptophan sufficiency signal that stimulates
12 mTOR: A novel IDO effector pathway targeted by D-1-methyl-tryptophan.
13 *Oncoimmunology* **2012**, *1*, 1460-1468.
14
15
16
17
18
19 7. a) Fallarino, F.; Grohmann, U.; You, S.; McGrath, B. C.; Cavener, D. R.; Vacca, C.;
20 Orabona, C.; Bianchi, R.; Belladonna, M. L.; Volpi, C.; Santamaria, P.; Fioretti, M. C.;
21 Puccetti, P. The combined effects of tryptophan starvation and tryptophan catabolites
22 down-regulate T cell receptor zeta-chain and induce a regulatory phenotype in naive T
23 cells. *J. Immunol.* **2006**, *176*, 6752-6761;
24
25
26
27
28
29
30 b) Munn, D. H.; Sharma, M. D.; Baban, B.; Harding, H. P.; Zhang, Y.; Ron, D.; Mellor, A.
31 L. GCN2 kinase in T cells mediates proliferative arrest and anergy induction in response
32 to indoleamine 2,3-dioxygenase. *Immunity* **2005**, *22*, 633-642.
33
34
35
36
37
38 8. a) Della Chiesa, M.; Carlomagno, S.; Frumento, G.; Balsamo, M.; Cantoni, C.; Conte, R.;
39 Moretta, L.; Moretta, A.; Vitale M. The tryptophan catabolite L-kynurenine inhibits the
40 surface expression of NKp46- and NKG2D-activating receptors and regulates NK-cell
41 function. *Blood* **2006**, *108*, 4118-4125;
42
43
44
45
46 b) Frumento, G.; Rotondo, R.; Tonetti, M.; Damonte, G.; Benatti, U.; Ferrara, G. B.
47 Tryptophan-derived catabolites are responsible for inhibition of T and natural killer cell
48 proliferation induced by indoleamine 2,3-dioxygenase. *J. Exp. Med.* **2002**, *196*, 459-468.
49
50
51
52
53
54
55
56
57
58
59
60

- 1
2
3 9. Sharma, M. D.; Baban, B.; Chandler, P.; Hou, D. Y.; Singh, N.; Yagita, H.; Azuma, M.;
4 Blazar, B. R.; Mellor, A. L.; Munn, D. H. Plasmacytoid dendritic cells from mouse tumor-
5 draining lymph nodes directly activate mature Tregs via indoleamine 2,3-dioxygenase. *J.*
6 *Clin. Invest.* **2007**, *117*, 2570-2582.
7
8
9
10
11
12 10. Manlapat, A. K.; Kahler, D. J.; Chandler, P. R.; Munn, D. H.; Mellor, A. L. Cell-
13 autonomous control of interferon type I expression by indoleamine 2,3-dioxygenase in
14 regulatory CD19+ dendritic cells. *Eur. J. Immunol.* **2007**, *37*, 1064-1071.
15
16
17
18
19 11. Holmgaard, R. B.; Zamarin, D.; Li, Y.; Gasmi, B.; Munn, D. H.; Allison, J. P.; Merghoub,
20 T.; Wolchok, J. D. Tumor-expressed IDO recruits and activates MDSCs in a Treg-
21 dependent manner. *Cell Rep.* **2015**, *13*, 412-424.
22
23
24
25
26 12. Mondal, A.; Smith, C.; DuHadaway, J. B.; Sutanto-Ward, E.; Prendergast, G. C.; Bravo-
27 Nuevo, A.; Muller, A. J. IDO1 is an integral mediator of inflammatory neovascularization.
28 *EBioMedicine* **2016**, *14*, 74-82.
29
30
31
32
33 13. Godin-Ethier, J.; Hanafi, L. A.; Piccirillo, C. A.; Lapointe, R. Indoleamine 2,3-dioxygenase
34 expression in human cancers: clinical and immunologic perspectives. *Clin. Cancer Res.*
35 **2011**, *17*, 6985-6991.
36
37
38
39
40 14. a) Greene, L. I.; Bruno, T. C.; Christenson, J. L.; D'Alessandro, A.; Culp-Hill, R.; Torkko,
41 K.; Borges, V. F.; Slansky, J. E.; Richer, J. K. A Role for tryptophan-2,3-dioxygenase in
42 CD8 T-cell suppression and evidence of tryptophan catabolism in breast cancer patient
43 plasma. *Mol. Cancer Res.* **2019**, *17*, 131-139;
44
45
46
47
48 b) Pilotte, L.; Larrieu, P.; Stroobant, V.; Colau, D.; Dolušić, E.; Frédérick, R.; De Plaen,
49 E.; Uyttenhove, C.; Wouters, J.; Masereel, B.; Van den Eynde, B. J. Reversal of tumoral
50
51
52
53
54
55
56
57
58
59
60

- 1
2
3 immune resistance by inhibition of tryptophan 2,3-dioxygenase. *Proc. Natl. Acad. Sci. U.*
4
5 *S. A.* **2012**, *109*, 2497-2502.
6
7
8 15. D'Amato, N. C.; Rogers, T. J.; Gordon, M. A.; Greene, L. I.; Cochrane, D. R.; Spoelstra, .
9
10 S.; Nemkov, T. G.; D'Alessandro, A.; Hansen, K. C.; Richer, J. K. A TDO2-AhR signaling
11
12 axis facilitates *anoikis* resistance and metastasis in triple-negative breast cancer. *Cancer*
13
14 *Res.* **2015**, *75*, 4651-4664.
15
16
17 16. Merlo, L. M.; DuHadaway, J. B.; Grabler, S.; Prendergast, G. C.; Muller, A. J.; Mandik-
18
19 Nayak, L. IDO2 modulates T cell-dependent autoimmune responses through a B cell-
20
21 intrinsic mechanism. *J. Immunol.* **2016**, *196*, 4487-4497.
22
23
24 17. a) Weng, T.; Qiu, X.; Wang, J.; Li, Z.; Bian, J. Recent discovery of indoleamine-2,3-
25
26 dioxygenase 1 inhibitors targeting cancer immunotherapy. *Eur. J. Med. Chem.* **2018**, *143*,
27
28 656-669;
29
30 b) Coletti, A.; Greco, F. A.; Dolciami, D.; Camaioni, E.; Sardella, R.; Pallotta, M. T.; Volpi,
31
32 C.; Orabona, C.; Grohmann, U.; Macchiarulo, A. Advances in indoleamine 2,3-
33
34 dioxygenase 1 medicinal chemistry. *Medchemcomm.* **2017**, *8*, 1378-1392.
35
36
37 18. a) Prendergast, G. C., Malachowski, W. P. DuHadaway, J. B.; Muller, A. J. Discovery of
38
39 IDO1 inhibitors: from bench to bedside. *Cancer Res.* **2017**, *77*, 6795-6811;
40
41 b) Röhrig, U. F.; Majjigapu, S. R.; Vogel, P.; Zoete, V.; Michielin, O. Challenges in the
42
43 discovery of indoleamine 2,3-dioxygenase 1 (IDO1) inhibitors. *J. Med. Chem.* **2015**, *58*,
44
45 9421-9437;
46
47 c) Dounay, A. B.; Tuttle, J. B.; Verhoest, P. R. Challenges and opportunities in the
48
49 discovery of new therapeutics targeting the kynurenine pathway. *J. Med. Chem.* **2015**, *58*,
50
51 8762-8782.
52
53
54
55
56
57
58
59
60

- 1
2
3
4
5
6
7
8
9
10
11
12
13
14
15
16
17
18
19
20
21
22
23
24
25
26
27
28
29
30
31
32
33
34
35
36
37
38
39
40
41
42
43
44
45
46
47
48
49
50
51
52
53
54
55
56
57
58
59
60
19. Yue, E. W.; Sparks, R.; Polam, P.; Modi, D.; Douty, B.; Wayland, B.; Glass, B.; Takvorian, A.; Glenn, J.; Zhu, W.; Bower, M.; Liu, X.; Leffet, L.; Wang, Q.; Bowman, K. J.; Hansbury, M. J.; Wei, M.; Li, Y.; Wynn, R.; Burn, T. C.; Koblisch, H. K.; Fridman, J. S.; Emm, T.; Scherle, P. A.; Metcalf, B.; Combs, A. P. INCB24360 (epacadostat), a highly potent and selective indoleamine-2,3-dioxygenase 1 (IDO1) inhibitor for immunoncology. *ACS Med. Chem. Lett.* **2017**, *8*, 486-491.
20. Soliman, H. H.; Antonia, S.; Sullivan, D.; Vanahanian, N.; Link, C. Overcoming coming tumor antigen anergy in human malignancies using the novel indeolamine 2,3-dioxygenase (IDO) enzyme inhibitor, 1-methyl-D-tryptophan (1MT). *J. Clin. Oncol.* **2009**, *27* (suppl 15; abstr 3004).
21. a) Kumar, S.; Waldo, J. P.; Jaipuri, F. A.; Marcinowicz, A.; Van Allen, C.; Adams, J.; Kesharwani, T.; Zhang, X.; Metz, R.; Oh, A. J.; Harris, S. F.; Mautino, M. R. Discovery of clinical candidate (1*R*,4*r*)-4-((*R*)-2-((*S*)-6-Fluoro-5*H*-imidazo[5,1-*a*]isoindol-5-yl)-1-hydroxyethyl)cyclohexan-1-ol (navoximod), a potent and selective inhibitor of indoleamine 2,3-dioxygenase 1. *J. Med. Chem.* **2019**, *62*, 6705-6733;
- b) Peng, Y. H.; Ueng, S. H.; Tseng, C. T.; Hung, M. S.; Song, J. S.; Wu, J. S.; Liao, F. Y.; Fan, Y. S.; Wu, M. H.; Hsiao, W. C.; Hsueh, C. C.; Lin, S. Y.; Cheng, C. Y.; Tu, C. H.; Lee, L. C.; Cheng, M. F.; Shia, K. S.; Shih, C.; Wu, S. Y. Important hydrogen bond networks in indoleamine 2,3-dioxygenase 1 (IDO1) inhibitor design revealed by crystal structures of imidazoleisoindole derivatives with IDO1. *J. Med. Chem.* **2016**, *59*, 282-293.
22. Crosignani, S.; Bingham, P.; Bottemanne, P.; Cannelle, H.; Cauwenberghs, S.; Cordonnier, M.; Dalvie, D.; Deroose, F.; Feng, J. L.; Gomes, B.; Greasley, S.; Kaiser, S. E.; Kraus, M.; Négrerie, M.; Maegley, K.; Miller, N.; Murray, B. W.; Schneider, M.; Soloweij, J.; Stewart,

- 1
2
3 A. E.; Tumang, J.; Torti, V. R.; Van Den Eynde, B.; Wythes, M. Discovery of a novel and
4 selective indoleamine 2,3-dioxygenase (IDO-1) inhibitor 3-(5-Fluoro-1*H*-indol-3-
5 yl)pyrrolidine-2,5-dione (EOS200271/PF-06840003) and its characterization as a potential
6 clinical candidate. *J. Med. Chem.* **2017**, *60*, 9617-9629.
7
8
9
10
11
12 23. a) Gangadhar, T. C.; Hamid, O.; Smith, D. C.; Bauer, T. M.; Waser, J. S.; Luke, J. J.;
13 Balmanoukian, A. S.; Kaufman, D. R.; Zhao, Y.; Maleski, J.; Leopold, L.; Gajewski, T. F.
14 Preliminary results from a phase I/II study of epacadostat (INCBO24360) in combination
15 with pembrolizumab in patients with selected advanced cancers. *J. Immunother. Cancer*
16 **2015**, *3* (suppl 2), 07;
17
18 b) A Phase 3 Study of Pembrolizumab + Epacadostat or Placebo in Subjects With
19 Unresectable or Metastatic Melanoma (Keynote-252 / ECHO-301). ClinicalTrials.gov
20 Identifier: NCT02752074. Last update: September 04, 2019 (accessed on Oct 23, 2019).
21
22
23
24 24. Long, G. V.; Dummer, R.; Hamid, O.; Gajewski, T.; Caglevic, C.; Dalle, S.; Arance, A.;
25 Carlino, M. S.; Grob, J.-J.; Kim, T. M.; Demidov, L. V.; Robert, C.; Larkin, J. M. G.;
26 Anderson, J.; Maleski, J. E.; Jones, M. M.; Diede, S. J.; Mitchell, T. C. Epacadostat (E)
27 plus pembrolizumab (P) versus pembrolizumab alone in patients (pts) with unresectable or
28 metastatic melanoma: Results of the phase 3 ECHO-301/KEYNOTE-252 study. 2018
29 ASCO Annual Meeting, *J. Clin. Oncol.* **2018**, *36*, (suppl 15; abstr 108).
30
31
32
33 25. a) Sondak, V. K.; Khushalani, N. Y. Echoes of a failure: what lessons can we learn? *Lancet*
34 *Oncol.* **2019**, *20*, 1037-1039;
35
36
37 b) Garber K. A new cancer immunotherapy suffers a setback. *Science* **2018**, *360*, 588;
38
39
40
41
42
43
44
45
46
47
48
49
50
51
52
53
54
55
56
57
58
59
60

- 1
2
3 c) Komiya, T.; Huang, C. H. Updates in the clinical development of epacadostat and other
4 indoleamine 2,3-dioxygenase 1 inhibitors (IDO1) for human cancer. *Front. Oncol.* **2018**,
5
6 8, 423-429.
7
8
9
10 26. Brochez, L.; Chevolet, I.; Kruse, V. The rationale of indoleamine 2,3-dioxygenase
11 inhibition for cancer therapy. *Eur. J. Cancer.* **2017** 76, 167-182.
12
13
14 27. a) Griglio, A.; Torre, E.; Serafini, M.; Bianchi, A.; Schmid, R.; Coda Zabetta G.;
15 Massarotti, A.; Sorba, G.; Pirali, T.; Fallarini, S. A multicomponent approach in the
16 discovery of indoleamine 2,3-dioxygenase 1 inhibitors: Synthesis, biological investigation
17 and docking studies. *Bioorg. Med. Chem. Lett.* **2018**, 28, 651-657;
18
19 b) Serafini, M.; Torre, E.; Aprile, S.; Massarotti, A.; Fallarini, S.; Pirali, T. Synthesis,
20 docking and biological evaluation of a novel class of imidazothiazoles as IDO1 inhibitors.
21
22 *Molecules* **2019**, 24, pii: E1874.
23
24 28. Fallarini, S.; Massarotti, A.; Gesù, A.; Giovarruscio, S.; Coda Zabetta, G.; Bergo, R.;
25
26
27
28
29
30
31
32
33
34
35
36
37
38
39
40
41
42
43
44
45
46
47
48
49
50
51
52
53
54
55
56
57
58
59
60
29. Sterling, T.; Irwin, J. J. ZINC 15--Ligand discovery for everyone. *J. Chem. Inf. Model*
2015, 55, 2324-2337.
30. a) FRED, version 3.0.0, OpenEye Scientific Software, Santa Fe, NM,
<http://www.eyesopen.com> (accessed on Oct 21, 2019);
b) McGann, M. FRED pose prediction and virtual screening accuracy. *J. Chem. Inf. Model.*
2011, 51, 578-596.
31. <https://www.emolecules.com> (accessed on Oct 21, 2019).

- 1
2
3 32. Duhr, S.; Braun, D. Why molecules move along a temperature gradient. *Proc. Natl. Acad.*
4
5 *Sci. U. S. A.* **2006**, *103*, 19678-19682.
6
7
8 33. Cavallo, G.; Metrangolo, P.; Milani, R.; Pilati, T.; Priimagi, A.; Resnati, G.; Terraneo, G.
9
10 The halogen bond. *Chem. Rev.* **2016**, *116*, 2478-2601.
11
12 34. a) Pick, R.; Bauer, M.; Kazmaier, U.; Hebach, C. Ammonia in Ugi reactions - four-
13
14 component versus six-component couplings. *Synlett* **2005**, *5*, 757-760;
15
16 b) Kazmaier, U.; Hebach, C. Peptide syntheses via Ugi reactions with ammonia. *Synlett*
17
18 **2003**, *11*, 1591-1594.
19
20
21 35. a) Schrödinger Release 2019-1: Desmond Molecular Dynamics System; D. E. Shaw
22
23 Research: New York, NY, 2019;
24
25 b) Maestro-Desmond Interoperability Tools 2019-1, Schrödinger, New York, NY, 2019.
26
27
28 36. Pirali, T.; Serafini, M.; Cargnin, S.; Genazzani, A. A. Applications of deuterium in
29
30 medicinal chemistry. *J. Med. Chem.* **2019**, *62*, 5276-5297;
31
32 b) Cargnin, S.; Serafini, M.; Pirali, T. A primer of deuterium in drug design. *Future Med.*
33
34 *Chem.* **2019**, *11*, 2039-2042.
35
36
37 37. a) Sharma, R.; Strelevitz, T. J.; Gao, H.; Clark, A. J.; Schildknecht, K.; Obach, R. S.; Ripp,
38
39 S. L.; Spracklin, D. K.; Tremaine, L. M.; Vaz, A. D. N.; Deuterium isotope effects on drug
40
41 pharmacokinetics. I. System-dependent effects of specific deuteration with aldehyde
42
43 oxidase cleared drugs. *Drug Metab. Dispos.* **2012**, *40*, 625-634;
44
45 b) Khan, A. J.; Misenko, S. M.; Thandoni, A.; Schiff, D.; Jhavar, S. R.; Bunting, S. F.;
46
47 Haffty, B. G. VX-984 is a selective inhibitor of non-homologous end joining, with possible
48
49 preferential activity in transformed cells. *Oncotarget* **2018**, *9*, 25833-25841;
50
51
52
53
54
55
56
57
58
59
60

- 1
2
3 c) Moslin, R.; Zhang, Y.; Wroblewski, S. T.; Lin, S.; Mertzman, M.; Spergel, S.; Tokarski,
4 J. S.; Strnad, J.; Gillooly, K.; McIntyre, K. W.; Zupa-Fernandez, A.; Cheng, L.; Sun, H.;
5 Chaudhry, C.; Huang, C.; D'Arienzo, C.; Heimrich, E.; Yang, X.; Muckelbauer, J. K.;
6 Chang, C.; Tredup, J.; Mulligan, D.; Xie, D.; Aranibar, N.; Chiney, M.; Burke, J. R.;
7 Lombardo, L.; Carter, P. H.; Weinstein, D. S. Identification of *N*-methyl nicotinamide and
8 *N*-methyl pyridazine-3-carboxamide pseudokinase domain ligands as highly selective
9 allosteric inhibitors of Tyrosine Kinase 2 (TYK2). *J. Med. Chem.* **2019**, *62*, 8953-8972.
- 10
11
12
13
14
15
16
17
18
19 38. a) Neoptolemos, J. P.; Palmer, D. H.; Ghaneh, P.; Psarelli, E. E.; Valle, J. W.; Halloran, C.
20 M.; Faluyi, O.; O'Reilly, D. A.; Cunningham, D.; Wadsley, J.; Darby, S.; Meyer, T.;
21 Gillmore, R.; Anthoney, A.; Lind, P.; Glimelius, B.; Falk, S.; Izbicki, J. R.; Middleton, G.
22 W.; Cummins, S.; Ross, P. J.; Wasan, H.; McDonald, A.; Crosby, T.; Ma, Y. T.; Patel, K.;
23 Sherriff, D.; Soomal, R.; Borg, D.; Sothi, S.; Hammel, P.; Hackert, T.; Jackson, R.;
24 Büchler, M. W. Comparison of adjuvant gemcitabine and capecitabine with gemcitabine
25 monotherapy in patients with resected pancreatic cancer (ESPAC-4): a multicentre, open-
26 label, randomised, phase 3 trial. *Lancet* **2017**, *389*, 1011-1024;
27
28 b) Cid-Arregui, A.; Juarez, V. Perspectives in the treatment of pancreatic adenocarcinoma.
29 *World J. Gastroenterol.* **2015**, *21*, 9297-9316.
- 30
31
32
33
34
35
36
37
38
39
40
41
42 39. Trovato, R.; Fiore, A.; Sartori, S.; Canè, S.; Giugno, R.; Cascione, L.; Paiella, S.; Salvia,
43 R.; De Sanctis, F.; Poffe, O.; Anselmi, C.; Hofer, F.; Sartoris, S.; Piro, G.; Carbone, C.;
44 Corbo, V.; Lawlor, R.; Solito, S.; Pinton, L.; Mandruzzato, S.; Bassi, C.; Scarpa, A.;
45 Bronte, V.; Ugel, S. Immunosuppression by monocytic myeloid-derived suppressor cells
46 in patients with pancreatic ductal carcinoma is orchestrated by STAT3. *J. Immunother.*
47 *Cancer* **2019**, *7*, 255-270.
48
49
50
51
52
53
54
55
56
57
58
59
60

- 1
2
3 40. Koblisch, H. K.; Hansbury, M. J.; Bowman, K. J.; Yang, G.; Neilan, C. L.; Haley, P. J.;
4
5 Burn, T. C.; Waeltz, P.; Sparks, R. B.; Yue, E. W.; Combs, A. P.; Scherle, P. A.; Vaddi,
6
7 K.; Fridman, J. S. Hydroxyamidine inhibitors of indoleamine-2,3-dioxygenase potently
8
9 suppress systemic tryptophan catabolism and the growth of IDO-expressing tumors. *Mol.*
10
11 *Cancer Ther.* **2010**, *9*, 489-498.
12
13
14
15 41. The PyMOL Molecular Graphics System, version 2.2.3, Schrödinger LLC, 2019.
16
17 42. QUACPAC, version 1.6.3.1; OpenEye Scientific Software: Santa Fe, NM,
18
19 <http://www.eyesopen.com> (accessed on Oct 21, 2019).
20
21
22 43. a) OMEGA, version 2.4.6; OpenEye Scientific Software: Santa Fe, NM,
23
24 <http://www.eyesopen.com> (accessed on Oct 21, 2019);
25
26 b) Hawkins, P. C.; Nicholls, A. Conformer generation with OMEGA: learning from the
27
28 data set and the analysis of failures. *J. Chem. Inf. Model.* **2012**, *52*, 2919-2936;
29
30 c) Hawkins, P. C.; Skillman, A. G.; Warren, G. L.; Ellingson, B. A.; Stahl, M. T. Conformer
31
32 generation with OMEGA: algorithm and validation using high quality structures from the
33
34 Protein Databank and Cambridge Structural Database. *J. Chem. Inf. Model.* **2010**, *50*, 572-
35
36 584.
37
38
39
40 44. Sugimoto, H.; Oda, S.; Otsuki, T.; Hino, T.; Yoshida, T.; Shiro, Y. Crystal structure of
41
42 human indoleamine 2,3-dioxygenase: catalytic mechanism of O₂ incorporation by a heme-
43
44 containing dioxygenase. *Proc. Natl. Acad. Sci. U. S. A.* **2006**, *103*, 2611-2616.
45
46
47 45. Banks, J. L.; Beard, H. S.; Cao, Y.; Cho, A. E.; Damm, W.; Farid, R.; Felts, A. K.; Halgren,
48
49 T. A.; Mainz, D. T.; Maple, J. R.; Murphy, R.; Philipp, D. M.; Repasky, M. P.; Zhang, L.
50
51 Y.; Berne, B. J.; Friesner, R. A.; Gallicchio, E.; Levy, R. M. Integrated modeling program,
52
53 applied chemical theory (IMPACT). *J. Comput. Chem.* **2005**, *26*, 1752-1780.
54
55
56
57
58
59
60

- 1
2
3 46. Toukmaji, A. Y.; Board, J. A. Ewald summation techniques in perspective: a survey.
4
5 *Comput. Phys. Commun.* **1996**, *95*, 73-92.
6
7
8 47. Zielkiewicz J. Structural properties of water: comparison of the SPC, SPCE, TIP4P, and
9
10 TIP5P models of water. *J. Chem. Phys.* **2005**, *123*, 104501-104506.
11
12 48. Martyna, G. J.; Klein, M. L.; Tuckerman, M. Nosé-Hoover chains: The canonical ensemble
13
14 via continuous dynamics. *J. Chem. Phys.* **1992**, *97*, 2635-2643.
15
16
17 49. Evans, D. J.; Holian, B. L. The Nose-Hoover thermostat. *J. Chem. Phys.* **1985**, *83*, 4069-
18
19 4074.
20
21 50. Fallarino, F.; Uyttenhove, C.; Boon, T.; Gajewski, T. F. Endogenous IL-12 is necessary for
22
23 rejection of P815 tumor variants in vivo. *J. Immunol.* **1996**, *156*, 1095-1100.
24
25
26 51. Fallarini, S.; Paoletti, T.; Battaglini, C. O.; Ronchi, P.; Lay, L.; Bonomi, R.; Jha, S.;
27
28 Mancin, F.; Scrimin, P.; Lombardi, G. Factors affecting T cell responses induced by fully
29
30 synthetic glyco-gold-nanoparticles. *Nanoscale* **2013**, *5*, 390-400.
31
32
33 52. Fallarini, S.; Paoletti, T.; Panza, L.; Lombardi, G. Alpha-galactosylceramide modulates the
34
35 induction of indoleamine 2,3-dioxygenase in antigen presenting cells. *Biochem.*
36
37 *Pharmacol.* **2008**, *76*, 738-750.
38
39
40
41
42
43
44
45
46
47
48
49
50
51
52
53
54
55
56
57
58
59
60

Table of Contents Graphic (TOC graphic)

